Aus der Klinik und Poliklinik für Orthopädie, Physikalische Medizin und Rehabilitation
Klinik der Ludwig-Maximilians-Universität München
Vorstand: Prof. Dr. med. Dipl.-Ing. Volkmar Jansson

Fracture Fixation of Complex Tibial Plateau Fractures

Dissertation
zum Erwerb des Doktorgrades der Humanbiologie
an der Medizinischen Fakultät der
Ludwig-Maximilians-Universität München

vorgelegt von

Shabnam Samsami

aus Teheran, Iran

2021

Mit Genehmigung der Medizinischen Fakultät

der Universität München

Berichterstatter:	Prof. Dr. Peter Müller
	Prof. Dr. Stefan Piltz
Mitberichterstatter:	PD. Dr. Carl Neuerburg
	PD. Dr. Stefan Grote
Mitbetreuung durch den promovierten Mitarbeiter:	Dr. Yan Chevalier
Dekan:	Prof. Dr. med. dent. Reinhard Hickel
Tag der mündlichen Prüfung:	26.04.2021

LMU LUDWIG-MAXIMILIANS-UNIVERSITÄT MÜNCHEN

Dean's Office
Faculty of Medicine

MMRS

Affidavit

Samsami, Shabnam
Surname, first name

Shabnam Samsami, C/O Institut für Biomechanik, BG Unfallklinik Murnau, Prof. Küntscher Str. 8
Street

82418 Murnau am Staffelsee
Zip code, town

Deutschland
Country

I hereby declare, that the submitted thesis entitled

Fracture Fixation of Complex Tibial Plateau Fractures

is my own work. I have only used the sources indicated and have not made unauthorised use of services of a third party. Where the work of others has been quoted or reproduced, the source is always given.

I further declare that the submitted thesis or parts thereof have not been presented as part of an examination degree to any other university.

Murnau am Staffelsee, 25.09.2020
Place, date

Sh. Samsami
Signature doctoral candidate

Contents

1. Abbreviations

AO	Arbeitsgemeinschaft für Osteosynthesefragen
Ant	Anterior
CAD	Computer-Aided Design
CT	Computer Tomography
DAAD	Deutscher Akademischer Austauschdienst
3D	Three Dimensional
2D	Two Dimensional
FE	Finite Element
FEA	Finite Element Analysis
Fracture C	Coronal Fracture
Fracture H	Horwitz Fracture
GPa	Giga Pascal
L	Lateral
LA	Lateral-Anterior
LC	Lateral-Central
LP	Lateral-Posterior
M	Medial
MA	Medial-Anterior
Max	Maximum
Min	Minimum
MM	Millimeter
MP	Medial-Posterior
MPa	Mega Pascal
MPC	Multi-Point Constraint Contacts
N	Newton
N/mm	Newton/Millimeter
OTA	Orthopaedic Trauma Association
Post	Posterior
R^2	R-Squared
RMSE	Root Mean Square Error
S	Single
TiAl6V4	Titanium 6% Aluminum 4% Vanadium

2. Publication List

➢ Publication I

The Effect of Coronal Splits on the Structural Stability of Bi-condylar Tibial Plateau Fractures: A Biomechanical Investigation

Shabnam Samsami, Robert Pätzold, Martin Winkler, Sven Herrmann, Peter Augat

Archives of Orthopedic and Trauma Surgery, Published online: 26 March 2020

DOI: 10.1007/s00402-020-03412-8, Volume 14, Pages 1719-1730

➢ Publication II

Finite Element Analysis of Bi-condylar Tibial Plateau Fractures to Assess the Effect of Coronal Splits

Shabnam Samsami, Sven Herrmann, Robert Pätzold, Martin Winkler, Peter Augat

Medical Engineering and Physics, Published online: 1 August 2020

DOI: 10.1016/j.medengphy.2020.07.026, Volume 84, Pages 84-95

3. Author Participations

In this section of the thesis, the contributions of authors, including me, are elaborated on for each publication. Moreover, the contribution forms, which were signed by coauthors for each paper, are attached in the following pages

3.1. Author Contributions for Publication I

In this publication (entitled: The Effect of Coronal Splits on the Structural Stability of Bi‑condylar Tibial Plateau Fractures: A Biomechanical Investigation), I, as a principle investigator, designed the load applicator and the protocol of the mechanical tests according to the physiological conditions. Also, I performed the mechanical tests and the data analyses, as well as wrote the manuscript. In this regard, Dr. Robert Pätzold, who developed the coronal fracture model based on the clinical data, prepared the artificial samples. Additionally, I consulted with him regarding the study design and interpretation of the results. Mr. Martin Winkler, as the leader of the mechanical test group in our institution, constructed the load applicator and the fracture template as well as helped me to execute the mechanical tests. He also advised me in the data analysis step. Furthermore, all study steps were discussed with Prof. Augat to profit from his professional guidance. When I, as the first and corresponding author, wrote the initial draft of this manuscript, sent it for all other authors for their revisions in which comments from Prof. Peter Augat were really helpful to improve the structure of this paper.

3.2. Author Contributions for Publication II

In this publication (entitled: Finite Element Analysis of Bi-condylar Tibial Plateau Fractures to Assess the Effect of Coronal Splits), I also was a principal researcher to construct

geometries of FE models, validate them based on the experimental conditions, as well as evaluate their numerical outcomes. Similar to the first publication, I was the first and corresponding author of this article too. In this regard, Dr. Sven Herrmann, as the leader of the numerical simulation group in our laboratory, advised me to conduct an appropriate validated FE study. Moreover, I benefited from his consultations to interpret and present the FE outcomes. Furthermore, Mr. Martin Winkler, as the leader of the mechanical test group in our institution, helped me with his advices regarding the experimental tests in order to validate the FE models. In addition, supervision of Prof. Augat assisted me in all research steps. The initial manuscript draft, which I wrote, was reviewed by all others, particularly Dr. Sven Herrmann and Prof. Peter Augat.

Cumulative Thesis

In accordance with § 4a Paras. 3 and 5 Examination Regulations for Dr. med., Dr. med. dent. and Dr. rer. biol. hum., as well as with § 7 Para. 4 Doctoral Degree Regulations for Dr. rer. nat. at the Medical Faculty
Please note: for each published article, a separate "Cumulative Thesis" form has to be submitted!

Shabnam Samsami

Name of doctoral candidate

Fracture Fixation of Complex Tibial Plateau Fractures

Title of dissertation

Title of article	The Effect of Coronal Splits on the Structural Stability of Bi-condylar Tibial Plateau Fractures: A Biomechanical Investigation
Title of journal	Archives of Orthopaedic and Trauma Surgery
Year	26 March 2020
Volume	140
Pages	1719-1730 DOI: 10.1007/s00402-020-03412-8

I hereby confirm that the extent of my contribution (content-related and volume) in the publication submitted is stated truthfully.

Sh. Samsami

Signature of doctoral candidate

By signing, the following **co-authors** confirm that:

- the extent of their contributions (content-related and volume) in the publications submitted and
- their agreement to the submission of the publications.

Name of co-author	Extent of contribution (content-related and volume)	Signature of co-author
1. Robert Pätzold	Developing the coronal fracture model based on clinical data; Sample preparation; Clinical consultation; Reviewing the manuscript	R. Pätzold
2. Martin Winkler	Manufacturing the load applicator and the fracture template; Helping in mechanical tests; Advising for data analysis; Consultations regarding outcomes; Reviewing the manuscript	M. Winkler
3. Sven Herrmann	Reviewing the manuscript	S. Herrmann
4. Peter Augat	Consultation in study design; Discussion about study outcomes; Advising for manuscript preparation; Reviewing the manuscript	P. Augat
5.		
6.		
7.		
8.		
9.		
10.		

Please list further authors on a separate page

Cumulative Thesis

In accordance with § 4a Paras. 3 and 5 Examination Regulations for Dr. med., Dr. med. dent. and Dr. rer. biol. hum., as well as with § 7 Para. 4 Doctoral Degree Regulations for Dr. rer. nat. at the Medical Faculty
Please note: for each published article, a separate "Cumulative Thesis" form has to be submitted!

Shabnam Samsami
Name of doctoral candidate

Title of dissertation

Title of article	Finite Element Analysis of Bi-condylar Tibial Plateau Fractures to Assess the Effect of Coronal Splits
Title of journal	Medical Engineering and Physics
Year	1 August 2020
Volume	84
Pages	84-95 DOI: 10.1016/j.medengphy.2020.07.026

I hereby confirm that the extent of my contribution (content-related and volume) in the publication submitted is stated truthfully.

Sh. Samsami
Signature of doctoral candidate

By signing, the following **co-authors** confirm that:

- the extent of their contributions (content-related and volume) in the publications submitted and
- their agreement to the submission of the publications.

Name of co-author	Extent of contribution (content-related and volume)	Signature of co-author
1. Sven Herrmann	Consultation in FEA steps including development of models, verification, validation, evaluation of results, and outcome interpretations; Advising in preparation of manuscript; Reviewing the manuscript	S. Herrmann
2. Robert Pätzold	Reviewing the manuscript	R. Pätzold
3. Martin Winkler	Consultation regarding experimental aspects of FE validation; Reviewing manuscript	M. Winkler
4. Peter Augat	Consultation in study design; Discussion about study outcomes; Advising for manuscript preparation; Reviewing the manuscript	P. Augat
5.		
6.		
7.		
8.		
9.		
10.		

Please list further authors on a separate page

4. Introduction

4.1. Clinical Background

Bi-condylar tibial plateau fractures, which account for 35% of all tibial plateau fractures, are considered as one of the most complex osseo-ligamentous traumas [1, 2]. This complexity is associated with multi-planar comminution as well as severe soft tissue injuries of the knee joint (Fig. 1) [1–4]. This type of fracture occurs mainly in males rather than females with a higher incidence in ages between 16 and 40 years old. Also, it usually results from high-energy accidents in which varus or valgus stresses along with axial loading contribute to injury [1, 2, 5]. The healing complications has been observed in 14% up to 42% cases of complex tibial plateau fractures [1, 6–10].

The most challenging type of bi-condylar tibial plateau fracture is that with a coronal split, thereby generating a posteromedial fragment as described initially by Barei et al [6, 7]. The reason for this complication is that the coronal fracture line could not be identified on bi-planar radiographs [11]. Moreover, fragmentation of the medial tibial condyle has been reported for almost 50% of bi-condylar tibial plateau fractures [1, 6, 7, 12]. Furthermore, when fixation of this crucial fragment is neglected, it may lead to some skeletal abnormalities including posterior subluxation of the femur during stance, an unstable femoral-tibial articulation, as well as a stiff arthritic knee [13]. Additionally, treatment aims of this trauma contains restoration of the limb alignment and the knee articular surface in order to recover patients to their normal activity levels [14]. Considering the preceding issues, a comprehensive characterization of the fracture site is required to provide an appropriate pre-surgery plan offering a biomechanically stable fixation, which reduces immobilization time [2, 15]. Accordingly, after the development of CT imaging that characterizes the 3D fracture morphology, the tibial plateau fracture has been an interesting

research topic in regard to fracture classification, fixation techniques, as well as treatment outcomes [16].

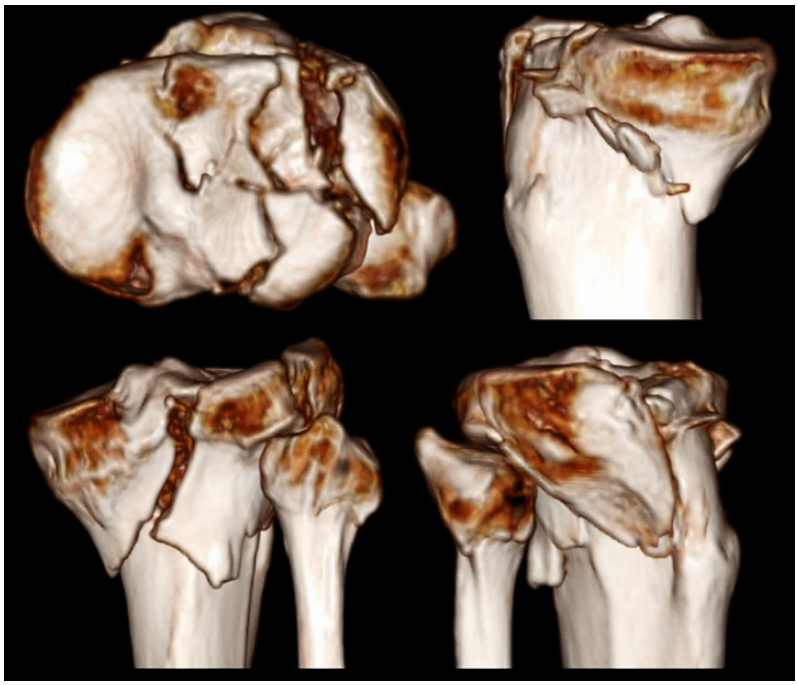

Fig. 1. Representative case of a bi-condylar tibial plateau fracture including the coronal split, adapted from Xie et al. 2020 [4].

Regardless of spread clinical and biomechanical studies, the ideal fixation method for this problematic injury is still questionable [1, 13, 17–21]. This is mainly because the established two-dimensional fracture classifications (Schatzker or AO/OTA) ignore the existence of the posteromedial fragment in their descriptions of bi-condylar tibial plateau fractures (Fig. 2) [3]. According to previous clinical investigations, using CT data altered the original category of almost 40% of the fractures which were initially classified based on the AO system [22]. In addition, employing CT scanning together with bi-planar radiographs changed not only the fracture grouping but also the surgery plan for more than 25% of patients [23]. MRI imaging, however, has not shown remarkable improvements for fracture evaluations [15]. Therefore, in addition to x-ray images, suitable 3D imaging techniques are required to recognize the coronal split as well as to determine the three-dimensional geometry of this complex fracture [15, 16].

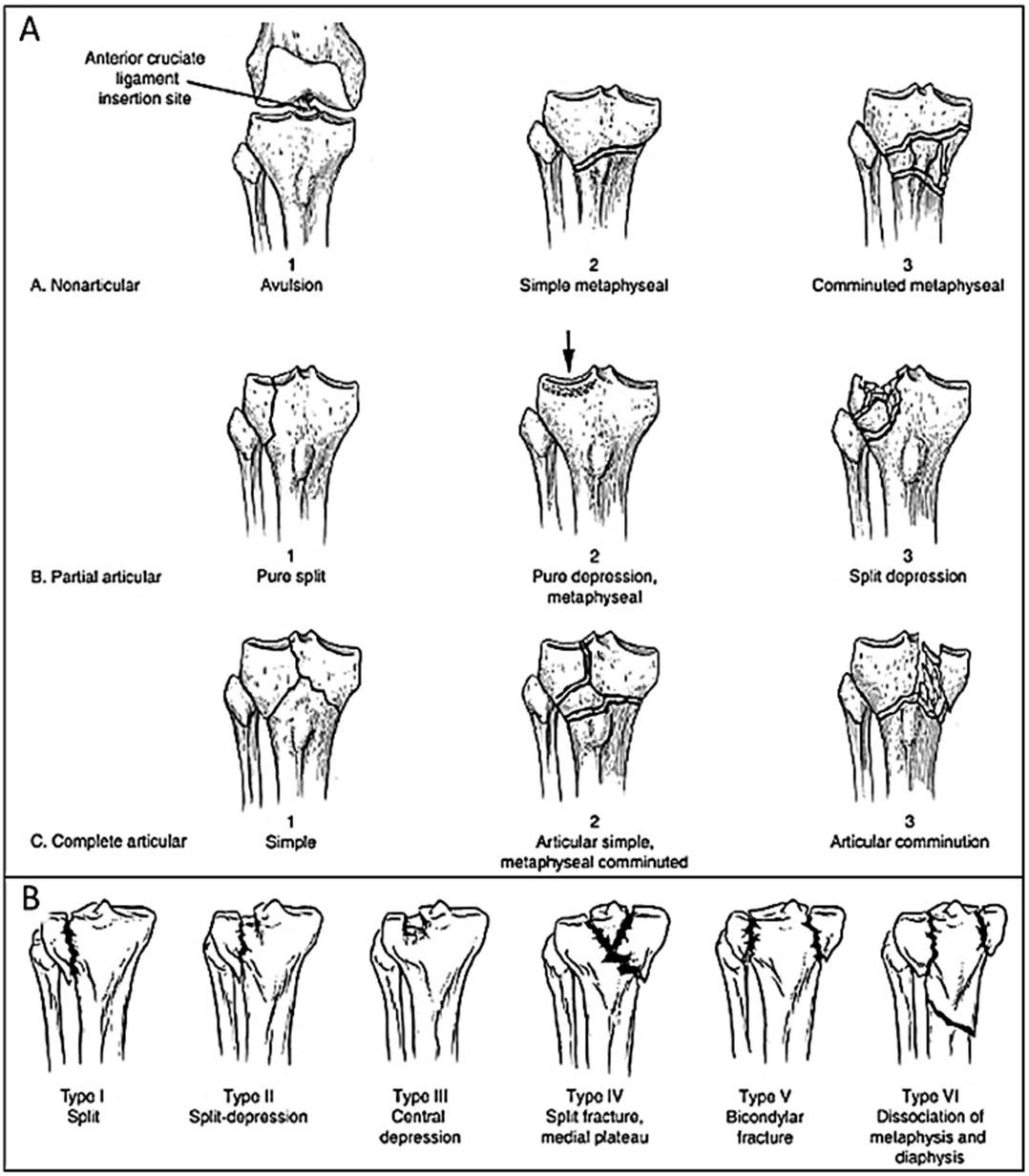

Fig. 2. Traditional fracture classifications for the tibial plateau fractures: A) The AO system, and B) The Schatzker classification, adapted from Berkson et al. 2006 [15].

The recent classifications developed by Luo et al. [24] or Krause et al. [25] have been focused on characterizing the posterior fragments of the tibial plateau fractures. The three-column concept introduced by Luo et al. has changed the understanding of fracture pattern and treatment strategies. It could not, however, describe the differences between split and depression fractures as well as between the posteromedial and posterolateral fractures [24]. The four-quadrant classification that distinguishes fragmentations of the posterolateral from posteromedial sections

of the tibial plateau was established by Chang et al [5]. Krause et al. proposed a ten-segment categorization in which the fracture locations are defined by considering axial CT images from the tibial articular surface to the 3-cm depth [25]. It should be noted that the three above-mentioned grouping did not provide detailed information about the mechanisms of injury associated with each fracture type [26, 27]. While planar images are practical for explaining the mechanisms of the injury, the exact location of the main fracture segments can be recognized by CT data [16, 27]. Consequently, unlike previous taxonomies which were based on either 2D or 3D imaging methods, Kfuri et al. recently revised the Schatzker classification using CT data combined with x-ray images. They developed a new fracture categorization in which 3D morphology of the fracture and the spatial location of the principle fracture planes are presented in addition to the injury mechanisms [16].

4.2. Biomechanical Background

Despite the high prevalence of the postoreomedial fragment and its critical role in preoperative planning, previous biomechanical experimental studies have not taken the presence of this fragment into account [11, 18-20, 28–36]. Although the recent fracture classifications have applied 3D imaging to describe the morphology of the posteromedial fragment, this concept has still not been transferred to biomechanical investigations. The traditional Horwitz model, which represents a Schatzker type VI fracture and ignores the coronal splits, has been widely utilized in the previous studies. This is yet another reason that the ideal fixation method for this kind of orthopaedic trauma is still under debate. Therefore, there is a great need to revise the traditional biomechanical fracture model by considering this crucial fracture fragment. In this regard, Yoo et al. recently executed the first mechanical tests for a Horwitz fracture model consisting of a posteromedial fragment [37]. However, their fracture model does not include all morphological

features of bi-condylar tibial plateau fractures. Our previous clinical study, based on the CT data of this complex trauma, revealed that for 97% of cases the sagittal lateral fracture line was observed in addition to their coronal major fracture line [1]. Accordingly, developing a fracture model based on the mentioned clinical observations concerning the morphology of this problematic injury is an essential step to find a biomechanically stable fixation method.

4.3. FEA Background

The finite element analysis (FEA) is implemented in the orthopaedic biomechanics field to develop implants or to help answer clinical questions by analyzing the parameters such as stresses or strains, which cannot be easily measured in experiments [38–40]. The essential steps in FEA are: 1) the verification to demonstrate that the FE model is free of numerical errors as well as 2) the validation to assess the reliability of FE simulations by comparing numerical outcomes with experimental data [39, 41, 42]. Afterwards, the predications of simulated bone-implant structures can be transferred to clinical applications. Importantly, the validated FE models can be used to answer clinical questions by evaluating variations of input parameters such as loading conditions, bone qualities, and material properties or even design factors of implants. Considering the costs and efforts required for the experimental explorations of these variables, FE modeling is an extremely adequate substitute for executing sensitive analyses in a multitude of scenarios [42].

There are two main shortcomings in previous FE studies regarding the bi-condylar tibial plateau fractures. The first major drawback was that the complex fracture morphologies were ignored, and only the simple fracture geometries were considered. Most importantly, these FE models were not validated in connection with experimental tests [43–47]. Although mechanical understanding of the influence of coronal splits on the load sharing within the bone-implant

structure can resolve the current debate about the ideal fixation method of this complex fracture, like biomechanical experimental investigations, previous numerical studies also did not take the posteromedial fragment into account. Therefore, there is a necessity to develop an FE model of this complex fracture based on clinically relevant morphology in order to provide mechanical knowledge for the proposal of an appropriate fixation method.

4.4. Objective of the Study

As mentioned in the previous sections, the standard fixation method for complex tibial plateau fractures is still controversial due to the disregard of the posteromedial fragment in previous biomechanical and numerical studies as well as in established fracture classifications. Therefore, a biomechanical investigation using a clinically relevant fracture model is required to resolve this issue. To address that, this study was designed in two parts which are elaborated on in the next sections as publication I and II, respectively. Part I, which applied mechanical tests on the synthetic bones, aimed to develop a biomechanical fracture model based on the clinical review of CT data as well as to assess the effect of coronal splits on the mechanical behaviour of the tibia-implant structure. Part II, which utilized the FE method, focused on the evaluation of stress distributions within the implant components to provide a detailed understanding about the influence of the coronal fracture line.

4.5. Publication I

4.5.1. Summary of Publication I

In this experimental publication, a biomechanical model of the bi-condylar tibial plateau fracture (Fracture C) including the coronal fracture line was developed and in terms of the

mechanical stability compared with the traditional Horwitz model (Fracture H) that disregarded the coronal split. Fracture models C and H were actualized using twelve specimens of the 4th generation tibias, and both of them were fixed with single lateral locked plating. The mechanical tests were performed under quasi-static and incremental cyclic loading until failure. The external force was transferred though a project-specific load applicator that consisted of femoral components of unilateral knee joint replacements to apply physiological pressure with a distribution of 60% on the medial tibial plateau surface and 40% laterally. Mechanical stability of the tibia-implant structures was compared between fracture models with respect to global stiffness, failure load, failure cycle, survival curve, as well as interfragmentary movements and relative rotations of fracture fragments.

The results of this publication showed that with the presence of a coronal split, the construct stiffness and the failure load of the bone-implant structure were reduced by 43% ($p = 0.013$) and 38% ($p = 0.016$), respectively. Considering the interfragmentary movement measurements, the coronal split resulted in the destabilization of the medial side of the tibia and a generation of joint incongruities which was resulted from the large relative displacement between the medial fragments and the tibial shaft as well as between the medial-anterior fragment and its posterior counterpart. Furthermore, the obtained results indicated that additional medial implantation is required due to the inadequacy of single plating with the lateral locking plate to stabilize this fracture.

In conclusion, this part of the study demonstrated that applying a fracture model based on the clinical morphology of bi-condylar tibial plateau fractures is fundamental for the biomechanical evaluations since the coronal articular fracture lines have remarkable effects on the mechanical stability of the tibia-implant constructs, particularly on the medial side.

4.6. Publication II

4.6.1. Summary of Publication II

This publication addressed the effect of the fracture morphology on stress distributions within the implant components by implementing the finite element analysis (FEA). For this purpose, two FE models corresponding to the coronal fracture model (Fracture C) consisting of the coronal split as well as the traditional Horwitz model (Fracture H) ignoring the coronal fracture line were developed. After the verification and validation of the FE models, stress distributions within the locking plates and screws were assessed.

For the validation purpose, Fractures C and H were realized on the synthetic tibial samples and fixed with the lateral locking plates to execute mechanical tests under the single and semi-physiological loading conditions. Global as well as local accuracies of the FE predictions were respectively assessed by regression analyses of the global axial stiffness and local displacements of optical markers, as well as by determining the root-mean-square errors (RMSE) for marker displacements of each fracture fragment and the percentage errors of the global axial stiffness [42, 48–50]. The validation step was initiated with calibrating the FE model of Fracture C under the simple and distributed loading conditions. First, the single loading case, in which an axial force was applied for the five different positions on the tibial plateau surface, was considered to evaluate the global stiffness and marker displacements for the FE model of Fracture C as well as to compare these numerical outcomes with the experimental ones. Following this calibration step, the load case was changed to a more realistic one by simulating a semi-physiological loading scenario similar to the experimental conditions. The FE model of Fracture C was also calibrated for this distributed loading condition. Subsequently to validate the FE simulations in the both loading cases, the same numerical assumptions were applied for the FE

model of Fracture H and then numerical and experimental outcomes were compared. It should be noted that due to the complexity of the semi-physiological load applicator including the distal femoral condyles, an initial sub-validation step under the single loading condition was executed. Eventually, under semi-physiological loading, the validated FE models of Fractures C and H were compared with respect to von-Mises stress distributions within the implant components, total deformations of tibia-implant constructs, as well as the load sharings between the medial and lateral tibial condyles.

The results of this publication illustrated that both fracture models were well validated, while FEA of Fracture C indicated superior agreements with the experimental outcomes than that of Fracture H. The assessments of the total deformation demonstrated that the coronal split increased the maximum total deformation of the tibia-implant structure by almost 73% in Fracture C than Fracture H, which caused higher relative displacement between the medial fragments and the tibial shaft. The evaluations of von-Mises stress distributions revealed that in comparison with Fracture H, the coronal split of Fracture C resulted in the alternation of the stress concentration areas from the middle part of the plate to the proximal section of the plate as well as a 61% increase in the peak stress of the kick-stand screw. In Fracture C, the proximal-dorsal and kick-stand screws were the main load-bearing parts, while in Fracture H the load was mainly transferred through the kick-stand screw. It should also be noted that the fracture morphology influenced the load sharing between the medial and lateral sides of the tibia. In Fracture H, the external load was shared almost equally on both tibial condyles. The lateral fragment of Fracture C, however, transferred 61% of the external load. 23% and 16% of the axial force were carried by the medial-anterior fragment and its posterior counterpart, respectively.

As a conclusion, this numerical section of the study also confirmed that the coronal fracture lines noticeably affected the stress distributions within the components of the locking

implants in addition to destabilizing the medial side of the tibia-implant constructs. Therefore, employing the clinically relevant FE model developed in this study is highly recommended for any numerical evaluations of bi-condylar tibial plateau fractures. Using this model can provide mechanical justification for selection of an ideal fixation method as well as for identification of the potential fatigue failure points in the lateral locking plates and screws.

4.7. Study Limitations

It is noteworthy to briefly consider the limitations of this study mentioned above as publications I and II. First, two fracture models were compared experimentally and numerically only under the axial and bending loading conditions since in most daily activities, the knee contact force is mainly applied in the axial direction. Moreover, the muscle forces were not taken into account for both the mechanical tests and the FE simulations. Furthermore, the ankle joint was simplified as a distal embedding cube. Additionally, the fourth-generation Sawbones were utilized instead of the human samples. Due to the constant geometry and the consistent mechanical properties, synthetic bones were selected to focus on the fracture morphology as the only study variable. Last but not least, both Fractures C and H were stabilized with single lateral plating which cannot appropriately reduce the movements of the medial fragments. This implantation was selected because it has been the most common plate used in the previous biomechanical studies investigating Fracture H. It can be postulated that the use of a more stable fixation method such as the double locked plating would noticeably decrease interfragmentary movements.

4.8. Conclusion of the Study and Future Perspective

To sum up, both experimental and numerical parts of the study suggest that the coronal articular fracture lines substantially affect both the mechanical response of tibia-implant structures, specifically on the medial side, as well as the stress distribution within the locking implant. Consequently, for the experimental and numerical evaluations of bi-condylar tibial plateau fractures, a clinically relevant fracture model should be utilized to compare different fixation methods or assess implant failures.

Having the outcome of this study in mind, the presented coronal fracture model should be implemented for future experimental researches to propose the best fixation method for this challenging orthopaedic trauma. In this regard, previous clinical studies have demonstrated that double plating fixation of the bi-condylar tibial plateau fractures consisting of the coronal splits provides adequate stability [2, 6, 13, 51]. This clinical recommendation, however, should be biomechanically investigated with the experimental tests based on the coronal fracture model. Therefore, the in-vitro mechanical tests on the cadaveric or synthetic tibial specimens can be executed to compare different configurations of the double plating such as the lateral locking plate combined with the medial locking plate located anteriorly or posteriorly.

Furthermore, the validated FE model of the bi-condylar tibial plateau fractures developed in this study can be utilized for future numerical sensitivity investigations. On the one hand, the fixation methods are primarily selected based on the surgeon's individual experience, disregarding comprehensive biomechanical assessments. On the other hand, the experimental investigations concerning available fixation options including all possible hardware configurations can be excessively complicated or even impossible. Therefore, the presented validated FE model of the bi-condylar tibial plateau fractures including coronal splits can be used

as a resource-efficient option to provide the biomechanical evaluations of different fixation methods. In order to find out the optimum plate position and implant design for this fracture type, distinctive fixation configurations of the medial and lateral locking plates can be analyzed regarding the effects of plate positions, implant designs, as well as screw orientations on the structural stability. It is worth mentioning that the current available fixation methods for bi-condylar tibial plateau fractures are not limited to the locking plates. External fixations, double compression buttress plates, or even intramedullary nailing can be offered as well [52]. Therefore, the coronal FE model established in this study can be also utilized to assess not only the different configurations of the locking plates but also distinct combinations of other fixation techniques. However, additional validation of the FE model is required, if non-locking implants are considered. Subsequently, the optimization process considering the implant positions and the geometrical variables of implants can be executed. Additionally, the effect of environmental variables such as the loading condition and the bone quality can be numerically estimated to suggest a stable fixation technique in the case of osteoporosis as well as for the variations of the external loads. Last but not least, clinical trial studies are also required to verify the biomechanical outcomes regarding the most stable fixation method.

5. Summary

Bi-condylar tibial plateau fractures with the highest frequency in 40-to-60-year-old patients accounts for 35% of all tibial plateau fractures. Surgical treatment of this fracture remains challenging due to the multi-planar articular comminution and the subsequent severe soft tissue injuries. Preoperative planning is meaningfully affected by recognition of the exact location of the fracture fragments, in particular the posteromedial fragment created by the coronal split. Despite the 50% incidence rate of this crucial fracture line, it has been disregarded in the established fracture classifications like the AO or Schatzker systems as well as in the previous biomechanical studies. For this reason, there is still a controversy regarding an ideal fixation strategy for the complex tibial plateau fractures. Therefore, through both experimental and the numerical investigations, this study aimed to develop a coronal fracture model based on the clinical data to ultimately address this concern. The experiments focused on comparison of the structural stability between the coronal fracture model and the traditional Horwitz model. The numerical simulations, which were established based on the validation of these fracture models, evaluated the effects of the fracture morphology on the stress distributions within the implant. Both study parts revealed that the coronal split remarkably reduced the global axial stiffness and displacement of the bone-implant structure, significantly destabilized the medial side of the tibia, as well as noticeably changed the stress distributions within the locking plates and screws. Furthermore, the lateral locking plate cannot adequately stabilize this fracture, and a double plating method including a supplemental medial plate is required. Consequently, it is highly recommended to apply the coronal fracture model of bi-condylar tibial plateau fractures for biomechanical tests, which aimed to compare different fixation methods, as well as for numerical studies, which focused on finding the optimum plate position, screw direction or plate design.

6. Zusammenfassung

Bicondyläre Tibiaplateaufrakturen machen 35% aller Tibiaplateaufrakturen aus, mit der höchsten Häufigkeit im Alter von 40-60 Jahren. Die chirurgische Behandlung dieser Fraktur bleibt aufgrund der multiplanaren Gelenkzertrümmerung sowie der nachfolgenden schweren Weichteilverletzungen eine Herausforderung. Das Erkennen der genauen Lage der Frakturfragmente wird bei der präoperative Planung, insbesondere durch die koronale Spaltung des entstandenen posteromedialen Fragments, erheblich beeinträchtigt. Trotz einer Inzidenzrate von 50% für diese kritische Frakturlinie wurde sie in den etablierten Frakturklassifikationen wie dem AO- oder Schatzker-System sowie in früheren biomechanischen Studien nicht berücksichtigt. Aus diesem Grund gibt es nach wie vor eine Kontroverse über eine ideale Fixationsstrategie für komplexe Tibiaplateaufrakturen. Daher zielte diese Studie, die aus experimentellen und numerischen Teilen besteht, darauf ab, auf der Grundlage der klinischen Daten ein koronales Frakturmodell zu entwickeln, um diesem Anliegen letztlich Rechnung zu tragen. Der experimentelle Teil konzentrierte sich auf den Vergleich der strukturellen Stabilität zwischen dem koronalen Frakturmodell und dem traditionellen Horwitz-Modell. Im numerischen Teil, der auf der Grundlage der Validierung dieser Bruchmodelle erstellt wurde, werden die Auswirkungen der Bruchmorphologie auf die Spannungsverteilungen innerhalb der Implantatkomponenten bewertet. Beide Teile dieser Studie zeigten, dass die koronale Bruchlinie die globale axiale Steifigkeit und Verschiebung der Knochen-Implantat-Struktur bemerkenswert reduziert, die mediale Seite der Tibia signifikant destabilisiert und die Spannungsverteilung innerhalb der Verriegelungsplatten und -schrauben merklich verändert hat. Außerdem kann die laterale Verriegelungsplatte diese Fraktur nicht ausreichend stabilisieren, so dass eine doppelte Verplattung einschließlich einer zusätzlichen medialen Platte erforderlich ist. Daher wird

dringend empfohlen, das koronale Frakturmodell für bikondyläre Frakturen des Tibiaplateaus anzuwenden, sowohl bei biomechanischen Tests, bei denen verschiedene Fixationsmethoden verglichen werden, als auch für numerische Studien, bei denen es darum geht, die optimale Plattenposition, Schraubenrichtung oder das optimale Plattendesign zu finden.

7. Publication I

Archives of Orthopaedic and Trauma Surgery (2020) 140:1719–1730
https://doi.org/10.1007/s00402-020-03412-8

TRAUMA SURGERY

The effect of coronal splits on the structural stability of bi-condylar tibial plateau fractures: a biomechanical investigation

Shabnam Samsami[1,2] · Robert Pätzold[2,3] · Martin Winkler[2] · Sven Herrmann[2,4] · Peter Augat[2,4]

Received: 11 December 2019 / Published online: 26 March 2020

Abstract

Introduction Surgical treatment of bi-condylar tibial plateau fractures is still challenging due to the complexity of the fracture and the difficult surgical approach. Coronal fracture lines are associated with a high risk of fixation failure. However, previous biomechanical studies and fracture classifications have disregarded coronal fracture lines.

Materials and methods This study aimed to develop a clinically relevant fracture model (Fracture C) and compare its mechanical behavior with the traditional Horwitz model (Fracture H). Twelve samples of fourth-generation tibia Sawbones were utilized to realize two fracture models with (Fracture C) or without (Fracture H) a coronal fracture line and both fixed with lateral locking plates. Loading of the tibial plateau was introduced through artificial femur condyles to cyclically load the fracture constructs until failure. Stiffness, fracture gap movements, failure loads as well as relative displacements and rotations of fracture fragments were measured.

Results The presence of a coronal fracture line reduced fracture construct stiffness by 43% ($p=0.013$) and decreased the failure load by 38% from 593 ± 159 to 368 ± 63 N ($p=0.016$). Largest displacements were observed at the medial aspect between the tibial plateau and the tibial shaft in the longitudinal direction. Again, the presence of the coronal fracture line reduced the stability of the fragments and created increased joint incongruities.

Conclusions Coronal articular fracture lines substantially affect the mechanical response of tibia implant structures specifically on the medial side. With this in mind, utilizing a clinically relevant fracture model for biomechanical evaluations regarding bi-condylar tibial plateau fractures is strongly recommended.

Keywords Bi-condylar tibial plateau fracture · Coronal fracture line · Horwitz fracture model · Coronal fracture model · Mechanical test · Interfragmentray displacement

Introduction

Bi-condylar tibial plateau fractures are challenging traumas due to their complex fracture geometry and accompanying soft tissue injury [1, 2]. These fractures mainly occur in young patients as a result of high-energy trauma and generally require open reduction and internal fixation [3, 4]. Healing complications for these fractures have been reported from 14% up to a staggering 42% [5–10]. The main goal of operative treatment is the patient's return to daily activity and functionality, which can be achieved through accurate reconstruction of the knee joint and the anatomical axes [2]. For planning and achieving suitable treatment, it has been recognized that providing a three-dimensional representation of the fracture by CT imaging plays a critical role [1, 11–14]. This is particularly important for articular fractures in the coronal plane as they are difficult to detect on bi-planar radiographs and complicated to

✉ Shabnam Samsami
biomechanik@bgu-murnau.de

1 Laboratory of Biomechanics and Experimental Orthopaedics, Department of Orthopedic Surgery, Physical Medicine and Rehabilitation, University Hospital of Munich (LMU), Campus Grosshadern, Munich, Germany

2 Institute for Biomechanics, Berufsgenossenschaftliche Unfallklinik, Murnau, Germany

3 Department of Trauma Surgery, Berufsgenossenschaftliche Unfallklinik, Murnau, Germany

4 Institute for Biomechanics, Paracelsus Medical University, Salzburg, Austria

characterize by two-dimensional fracture classifications such as Schatzker or AO/OTA [15]. The AO/OTA and Schatzker classifications are the most common taxonomies of tibial plateau fractures due to their simplicity, while they disregard injury patterns observed in the third dimension [16].

The clinical relevance of these coronal fractures was identified by Barei et al. as a fracture pattern that separates a posteromedial fragment from the tibial plateau [11] and which has a prevalence of almost 50% in complex tibial plateau fractures [1, 11, 17]. The detection of this fracture line is clinically important because lateral locking plates, which are a common fixation method for this fracture, may not effectively stabilize the posteromedial fragment and supplemental implants may be required [5, 6, 11, 18–20]. To adequately describe the personality of complex tibia plateau fractures, various three-dimensional classification schemes such as the "three-column" concept were developed to refine the traditional planar classifications as a guide for surgical planning [21]. Recently, an extension of the Schatzker classification was introduced in which the fracture type and the mechanism of injury were described based on plain radiographs as well as CT data were utilized to provide complemental third-dimensional information about the location of the main fracture planes [22]. Although the clinical relevance of the posteromedial fragment and the dependency of treatment plans on identifying fracture locations has been recognized, there is still a lack of understanding regarding the biomechanical implications of the posteromedial fragment, in particular with respect to its adequate stabilization [1]. Previous biomechanical studies on bicondylar tibial plateau fractures have largely been based on the model developed by Horwitz et al. [23] to simulate a Schatzker Type VI fracture. As this model is based on a coronal projection of the fracture, it completely ignores any coronal fracture lines and thus the presence of a posteromedial fragment. Yet, it remains the most frequently employed biomechanical model [23–35] on which recommendations for fracture fixation of complex tibia plateau fractures are based upon.

Due to the aforementioned negligence of articular fracture lines, establishing a clinically relevant, biomechanical fracture model is required to resolve controversies regarding the ideal fixation method for this complex trauma. The aim of this study was to develop a biomechanical model for bicondylar tibial plateau fractures, which incorporates a coronal fracture line. We hypothesized that our novel coronal fracture model would exhibit inferior mechanical stability compared to the traditional Horwitz model.

Materials and methods

This biomechanical study was performed on synthetic bone analogues which were osteotmized to produce two different fracture models: the traditional Horwitz fracture model (Fracture H) and a novel fracture which was based on a systematic review of CT images [1] and included a coronal fracture line (Fracture C). The fracture models were fixed with locked plating constructs and were quasi-statically as well as cyclically loaded to determine the mechanical stability as measured by stiffness, fragment movement and failure loads.

Sample preparation

Twelve synthetic tibial bones (#3406 left large tibia, 4th Generation, Sawbones, Malmö, Sweden) were prepared with identical osteotomies using a custom-made jig and an oscillating saw. For Fracture H, the central triangle of the proximal tibia was removed to mimic an unstable fracture situation [23, 34]. The first cutting line started from the intercondylar eminence and ended at a point on the lateral cortex located 4 cm distally from the lateral plateau. The medial cut was made from the intercondylar eminence to a point on the medial cortex positioned 6 cm distally from the medial plateau. A final cut was made to connect the lateral and medial cortex points (Fig. 1a). The coronal fracture model (Fracture C) consisted of coronal and sagittal articular fracture lines. The coronal fracture line was made in the center part of the medial tibial plateau in the superior view. The sagittal fracture line split the lateral plateau and intercondylar eminence of the tibia in the transverse plane. Then, lateral and medial cuts were made from the Tuberculum intercondylare laterale to the lateral cortex at 4 cm and on the medial cortex at 6 cm distal from the tibial plateau. The final osteotomy connected the lateral and medial splits and the central triangle of the bone from the proximal tibia was removed (Fig. 1b).

Both fracture types were fixed with titanium locking plates (AxSOS Proximal Lateral Tibia Plate, left, six-hole length, Stryker, Selzach, Switzerland) by an experienced orthopedic trauma surgeon according to the manufacturers' recommendations using locking self-taping screws of 4-mm diameter (four articular screws including two 80-mm screws for proximal-posterior and proximal-inferior plate holes, 85 and 70-mm screws for proximal-middle and proximal-anterior plate holes, respectively, one kick-stand screw with 75-mm length as well as six shaft screws with length between 20 and 32 mm). A 3D-printed template was used to ensure that implants were inserted identically in all specimens (Fig. 2).

Experimental setup

The distal end of the tibia was embedded in an aluminum box to a depth of 50 mm using a three-component casting resin (RenCast FC 53 A/B + Füller DT 082, Gößl + Pfaff GmbH, Karlskron/Brautlach, Germany). This box was clamped to the base of the testing machine (Instron E3000,

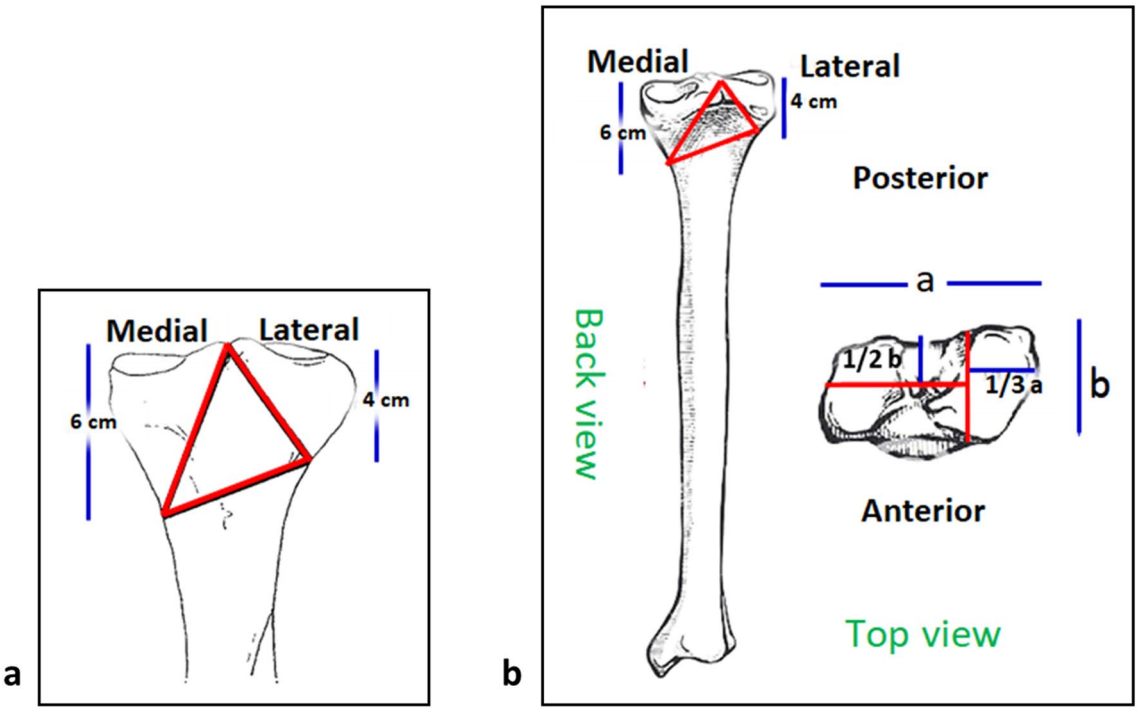

Fig. 1 **a** Fracture H according to the schematic drawing of Horwitz et al. [23] and [34]. **b** Fracture C developed based on clinically relevant fracture lines [1]

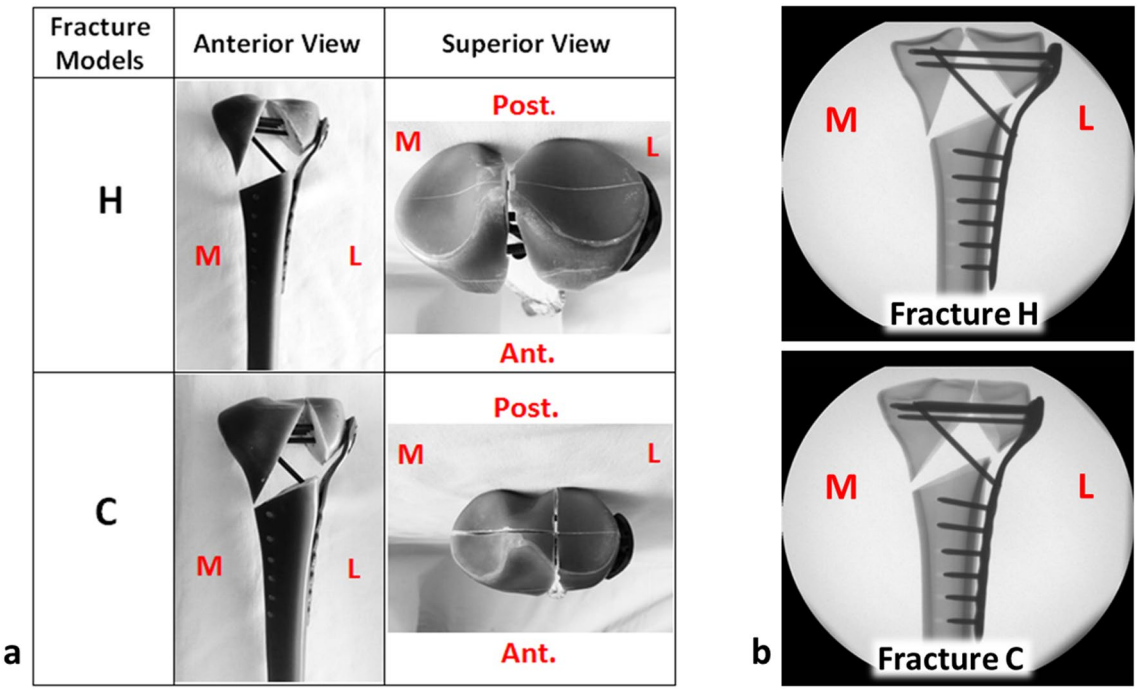

Fig. 2 **a** Prepared samples for fracture models H and C. **b** Anterior–posterior X-ray of prepared specimens for each fracture model

Instron Structural Testing, High Wycombe, UK) to rigidly fix samples in a vertical position. Loading was introduced through artificial femur condyles of unilateral knee replacements which were embedded in polyurethane blocks. These blocks were attached to the actuator of the testing machine with a hinge joint, which allowed the femur condyles to tilt in the frontal plane and balance the movement of the tibial head (Fig. 3a). The testing machine included a Dynacell load cell (Capacity of ± 10 kN, ISO 7500-1 Class 1, Instron Structural Testing, High Wycombe, UK) and data logging software (Instron Console V8.4 and Instron Wave Matrix V1.5, High Wycombe, UK).

To simulate physiological loading conditions, femoral condyles were positioned in such a way that the equidistant point and the axis of the testing machine were not aligned, so the applied load was distributed 40% laterally and 60% medially on the tibial plateau (Fig. 3b) [35, 36].

Loading scenario

At the beginning of loading, six static displacement-controlled ramps (10 mm/min) up to 250 N were performed. The first three static ramps allowed the samples to settle, while the second three cycles were used to measure the initial stiffness of the tibia-implant constructs. Afterwards, constructs were cyclically loaded with a sinusoidal axial load (2 Hz) between the lower level of 20 N and an incrementally increasing upper load level. The upper load level started at 250 N and was increased stepwise by 50 N every 500 cycles to mimic increasing levels of weight bearing. Additionally, static measurements were taken at maximum loads before and after increments of 500 cycles (Fig. 4).

All specimens were loaded until mechanical failure (i.e., Sawbone breakage, gap closure on the medial side of the tibia, or implant failure). With a retrospective analysis of ARAMIS data, the clinical failure point was defined as ≥ 5° relative rotations of fracture fragments, ≥ 5-mm fracture gap displacements for medial- or lateral-shaft gaps, or ≥ 2-mm displacements of articular gaps on the tibial plateau, whichever occurred first [37, 38].

Interfragmentary movement analysis

To track the relative displacement of fracture fragments, an optical measurement system (ARAMIS 5M, GOM GmbH, Braunschweig, Germany) with measurement error < 0.1% and 2% for relative translational and rotational movements, respectively [39], was utilized. ARAMIS system consists of data capturing and analysis software (GOM Correlate Professional 2018, GOM GmbH, Braunschweig, Germany) that utilizes stereo-image based techniques to evaluate the coordinates and displacements of objects with image correlation from point marker or stochastic pattern recognition. The global coordinate system was defined using computer-aided design (CAD) files of the tibial shaft and the best-fit algorithm included in the GOM Correlate software. Then,

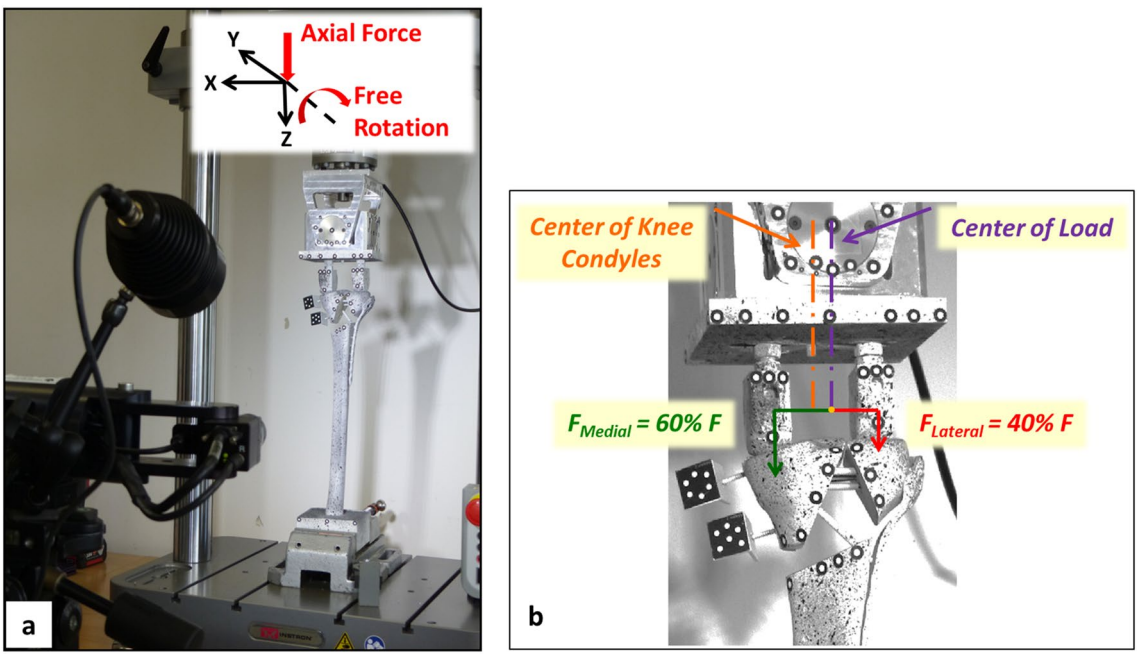

Fig. 3 **a** Experimental setup for mechanical test in which the highlighted local coordinate system indicates degrees of freedom for the load applicator. **b** Load applicator and more details about load distribution. Also, the marker placements and the spray pattern for image detection can be seen

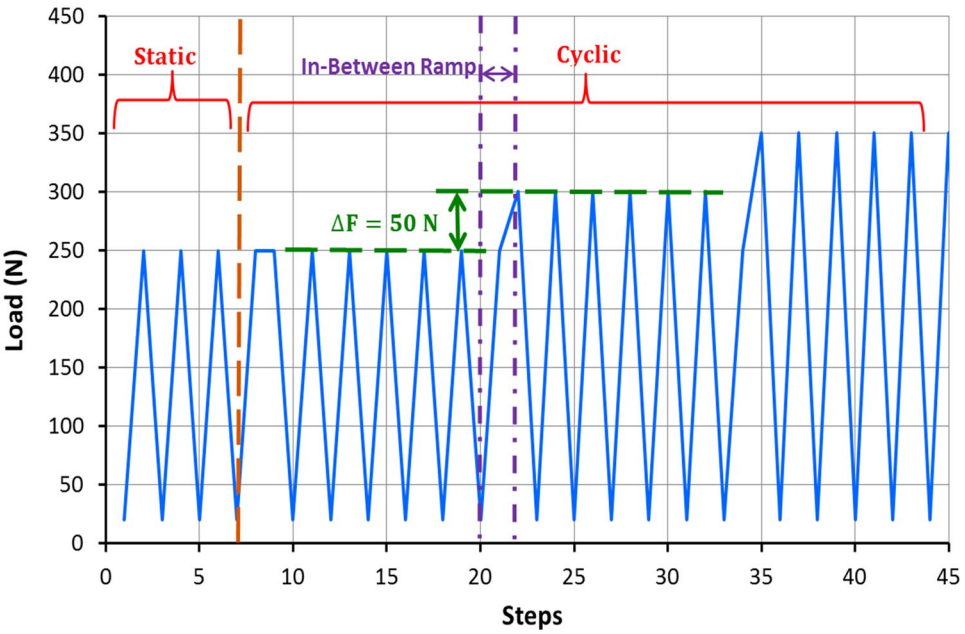

Fig. 4 Force-steps curve that indicates loading scenario includes static and incremental cyclic

CAD files of other fracture fragments were virtually matched with the corresponding surface and point components to track relative displacements between fracture parts (Fig. 5a).

Interfragmentary movements and the relative rotation of fracture segments with respect to the tibial shaft were analyzed to elucidate displacement of fracture fragments. All kinematic data were reported in the anatomic coordinate system in which *x*, *y* and *z* axes indicate frontal, sagittal and longitudinal directions, respectively. Moreover, the axial displacement of the loading center was evaluated in the loading coordinate system (Fig. 5b). Every 100 cycles, ARAMIS pictures were taken at the maximum and minimum loads to measure the elastic and plastic deformations of the construct, respectively. Additionally, a static measurement at the point of maximum load before and after each 500 cycles was made to track the elastic deformation of the specimens. To evaluate the movement of the fracture fragments during loading, a pair of points was considered in the center of each gap to measure changes in the relative distances of individual gaps (Fig. 6).

Measurement outputs

From recorded data, the following parameters were evaluated:

1. Static construct stiffness (N/mm), defined as load changes between 20 and 250 N divided by the corresponding axial displacement of the loading center in the static step.
2. Cyclic construct stiffness (N/mm), which was calculated by considering in-between ramps between cyclic steps and dividing load changes between 20 and 250 N by the corresponding axial displacement of the loading center.
3. Interfragmentary displacement (mm), determined as relative movement between individual fracture gaps and reported for static loading as well as after 2500 cycles at the 500 N force corresponding to 20% of maximum knee contact force [40].
4. Rotations of fracture fragments around the three anatomical axes with respect to the tibial shaft (degree), which were evaluated at the maximum load levels during cyclic steps.
5. Failure load (N) and failure cycles that determine the load and the number of cycles where the samples exceeded clinical failure criteria.
6. Survival curves as a comparison between fracture models for level of load tolerance regarding clinical failure.

Statistical analysis

Independent *t* tests were applied to compare mechanical parameters between the two fracture models. The assumptions of independent *t* test consisting of independence, interval scale, normal distribution, as well as homogeneity of variances (Levene's test) were evaluated for both fracture groups. Normal distributions of data were assessed with Shapiro–Wilk's test ($p > 0.05$) as well as visual inspection of the histogram, normal *Q*–*Q*, and box plots. For the fatigue tests, Kaplan–Meier survival analyses with log-rank tests were executed (IBM SPSS Statistics 19, Chicago, IL, US).

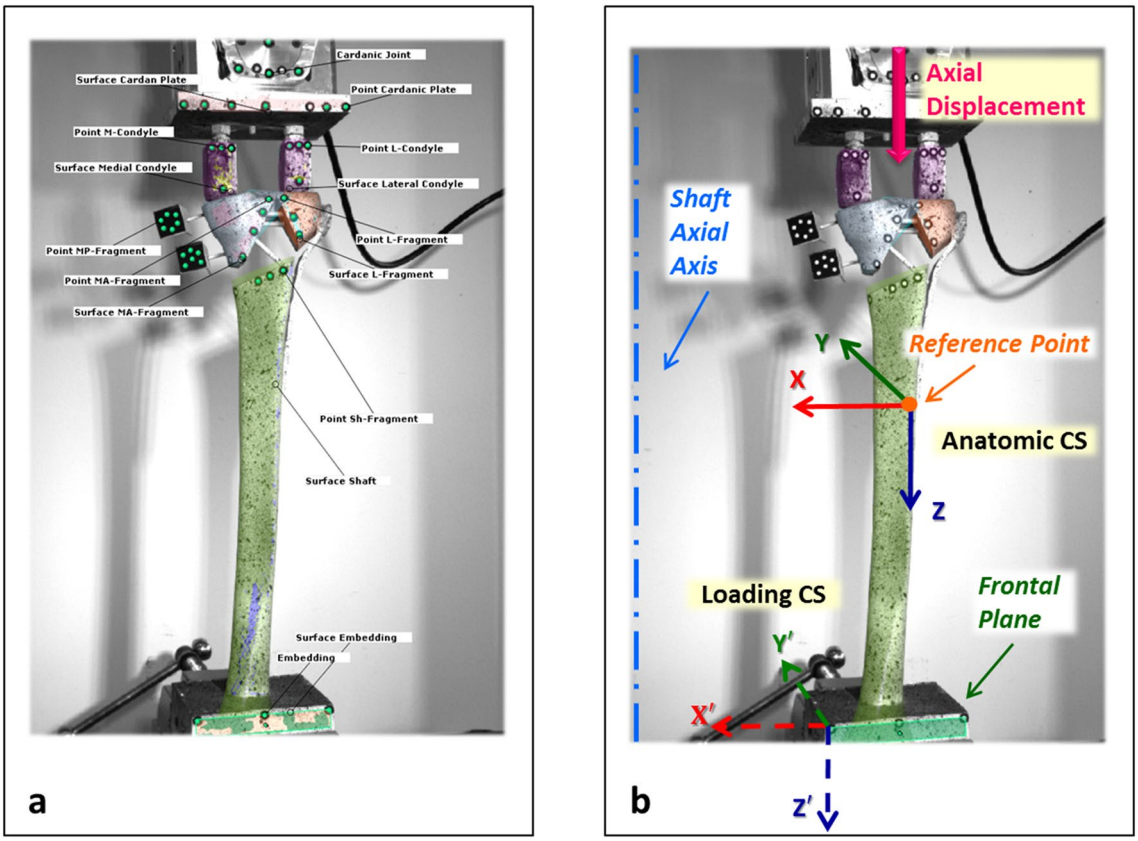

Fig. 5 **a** A general view for the defined markers and surfaces as well as fitted CAD files in GOM Correlate software. **b** Axial displacement of the loading point highlighted with an arrow as well as details of the loading and anatomic coordinate systems

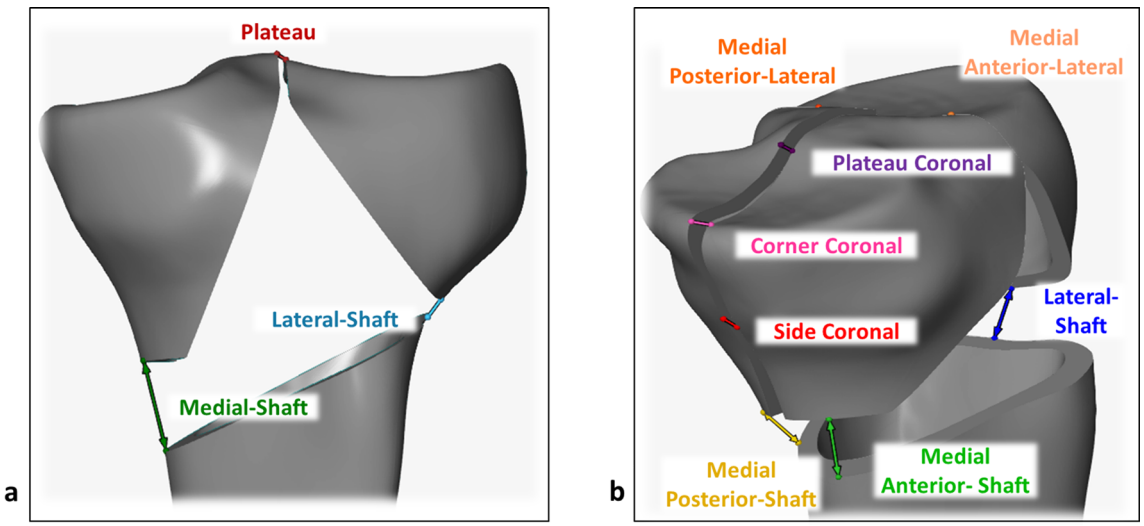

Fig. 6 Positions for measurement of interfragmentary movements. **a** Fracture H: medial-shaft, lateral-shaft, and plateau gaps. **b** Fracture C: medial anterior-shaft, medial posterior-shaft, lateral-shaft, side coronal, corner coronal, plateau coronal, medial anterior-lateral, and medial posterior-lateral gaps

Table 1 Comparing mechanical properties between Fractures H and C (mean ± standard deviation, $n = 6$)

	Static stiffness (N/mm)	Failure load (N)	Failure cycles
Fracture H	304 ± 95	593 ± 159	3517 ± 1493
Fracture C	172 ± 50	368 ± 63	1433 ± 656
p	0.013	0.016	0.017

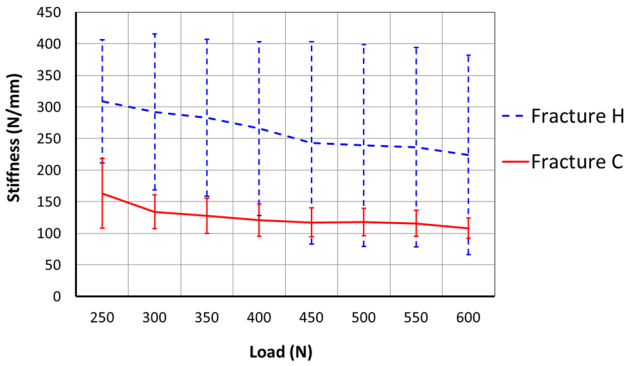

Fig. 7 Cyclic stiffness for both fracture configurations (mean ± standard deviation, $n = 6$)

Results

In static loading, the axial stiffness of Fracture C was 43% lower than that of Fracture H (Table 1, $p = 0.013$). During cyclic steps, depending on the load level, Fracture C was on average 47–55% laxer than Fracture H (Fig. 7).

To elucidate the effect of the coronal fracture line on fragment stability, relative displacements and rotations were evaluated for the key fracture fragments. Although fragment displacements were evaluated during the whole cyclic testing procedure, we report the displacements after 2500 cycles at the 500-N load level corresponding to 20% of the maximum knee contact force (Fig. 8). For both Fractures H and C, displacements on the medial sites were predominantly in the longitudinal direction followed by frontal and sagittal displacements. In particular, displacement at the medial anterior-shaft gap of Fracture C was almost exclusively in longitudinal direction and exceeded the 5-mm clinical failure criteria (Fig. 8a). Both coronal gaps of Fracture C were mainly displaced in the sagittal direction followed by the longitudinal and frontal movements. The average sagittal displacements exceeded the 2-mm failure criteria at both locations in the plateau (Fig. 8b).

As the displacement measurements indicated that the medial-anterior and medial-posterior fragments of Fracture C moved in different directions, relative rotations of these fragments were analyzed (Fig. 9). Analysis of the sagittal rotation revealed that the coronal split mainly destabilized the medial-anterior fragment which showed larger rotations compared to its corresponding posterior one as well as the whole medial segment of Fracture H (Fig. 9a). Regarding the frontal rotation, unlike the movement of the medial segment in Fracture H, the coronal split resulted in reversing the rotation of both medial fragments toward the posterior direction (Fig. 9b). Finally, for the longitudinal rotation, the coronal split destabilized the medial-posterior fragment, demonstrating a more than threefold increase in internal rotation when compared to its anterior counterpart as well as the medial component of Fracture H (Fig. 9c). For both Fractures H and C, interfragmentary

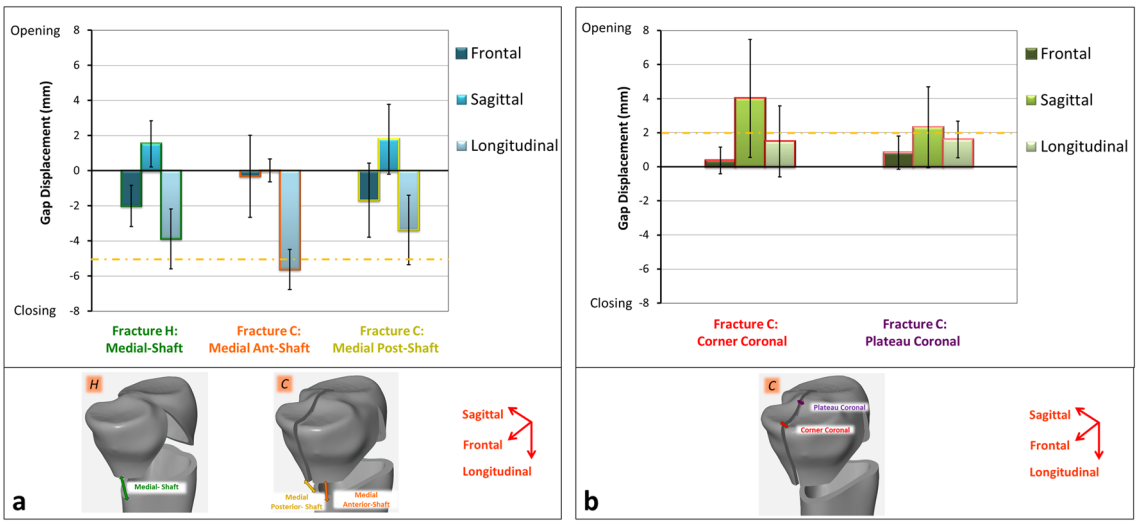

Fig. 8 Interfragmentary displacements at 500-N cyclic load after 2500 cycles. **a** Medial-shaft gaps of Fractures H and C. **b** Coronal gaps of Fracture C. The dash-dotted lines depict clinical failure criteria

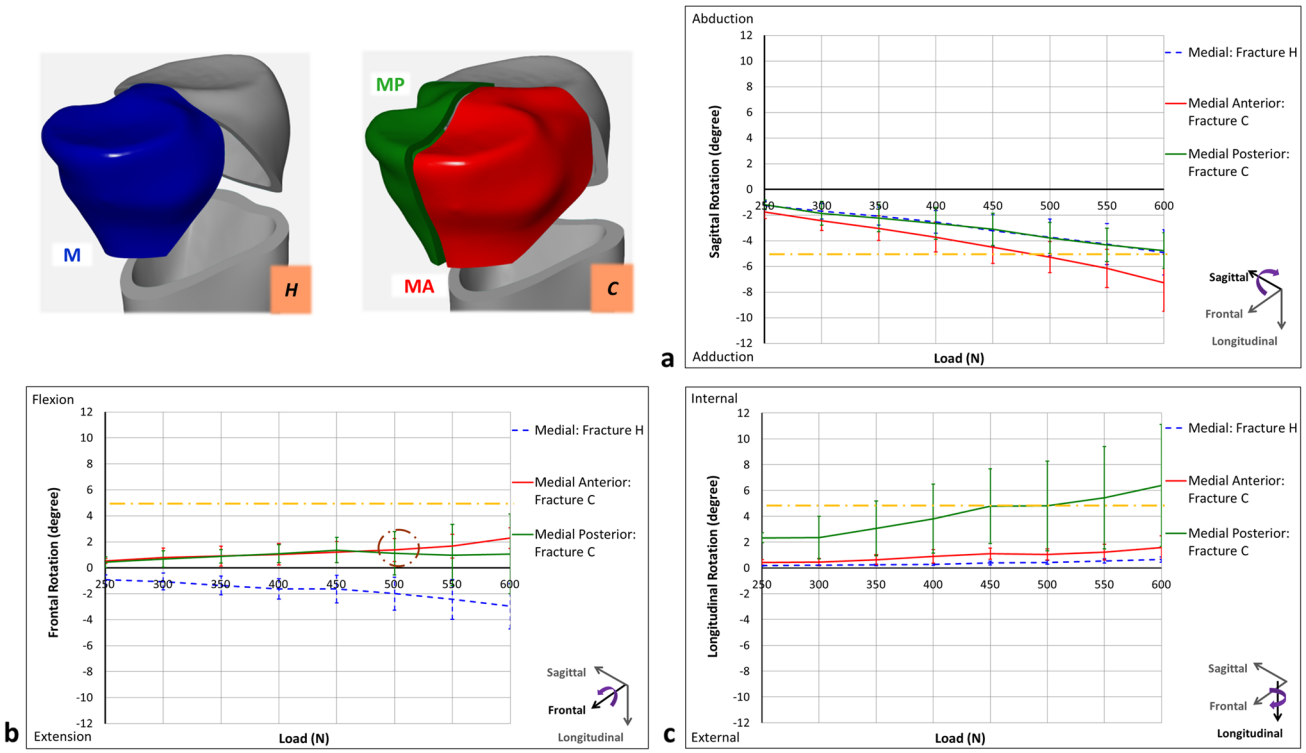

Fig. 9 Relative rotations of the medial fragments for Fractures H and C with respect to the tibial shaft. **a** Sagittal rotation. **b** Frontal rotation (dash-dotted circle indicates destabilization of diagonal screw). **c** Longitudinal rotation. Dash-dotted lines demonstrate clinical failure criteria

movements of the lateral-shaft and medial–lateral gaps were almost negligible compared to those of the medial-shaft and coronal gaps. Moreover, the movements of these two gaps and relative rotations of lateral fragments were similar in both fracture models.

Shapiro–Wilk's test ($p > 0.05$) as well as visual inspection of the histogram, normal Q–Q, and box plots indicated that for both Fractures H and C, the parameters of mechanical stability (i.e., static stiffness, failure load, and failure cycles) were approximately normally distributed. According to the clinical failure criteria, Fracture C failed earlier and at lower load levels compared to Fracture H which tolerated 60% higher load levels ($p = 0.016$). Failure cycles of Fracture H samples were almost 2.5 times that of Fracture C (Table 1, $p = 0.017$). The survival analysis revealed that the survival rate of Fracture H was almost 2.5 times that of the Fracture C group. While none of the Fracture C samples survived the clinical failure criteria until 2500 cycles or 500-N load, half of Fracture H specimens survived 2500 cycles (Fig. 10, $p = 0.006$).

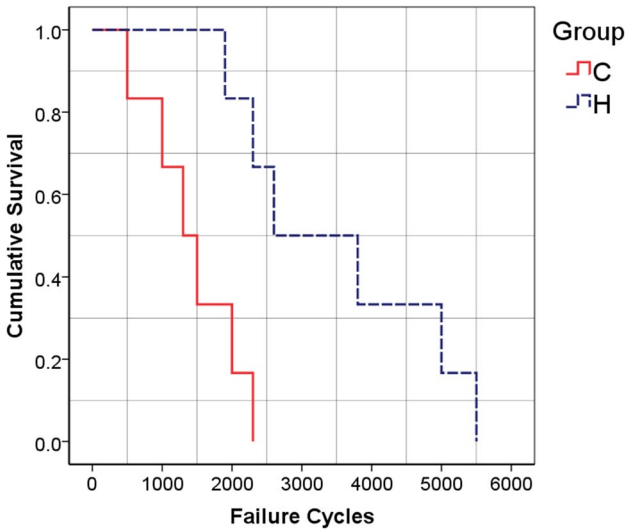

Fig. 10 The survival curves for Fractures H and C

Discussion

Articular fracture lines in complex tibial plateau fractures which result in a coronal split have been widely ignored in previous biomechanical studies and fracture classifications [11]. Thus, we developed a coronal fracture model based on 3D fracture morphologies [1] and assessed this model biomechanically. Our study revealed that the presence of a coronal split generates an unstable posteromedial fragment which is inadequately stabilized with unilateral plating from the lateral aspect. The coronal split reduced the stiffness and

decreased the strength of fracture fixation and resulted in increased fragment displacements during loading.

The biomechanical assessments revealed that Fracture H was almost two times stiffer and tolerated 1.5 and 2.5 times higher load level and cycles, respectively, as compared to Fracture C (Table 1). Also, the survival rate of the Fracture H group was nearly 150% higher than that of Fracture C. Thus, the coronal fracture line remarkably destabilized the fracture fixation construct.

To further understand the effects of coronal fracture lines, the rotations of fracture fragments relative to the tibial shaft and interfragmentary displacements were analyzed. Interfragmentary movements (especially on the articular surfaces) are considered an important clinical parameter because an articular subsidence of more than 2–3 mm remarkably increases knee joint pressure and may result in osteoarthritis [41, 42]. Moreover, malalignment is an important factor in evaluating treatment outcomes of tibia plateau fractures and rotations of joint lines more than 5° are considered fixation failure [37, 43, 44]. Thus, interfragmentary displacements of the medial and plateau fracture gaps were analyzed to assess a risk of bone non-union and osteoarthrosis, respectively. The relative rotations of medial fracture fragments with respect to the tibial shaft are also indicative of limb malalignment. To the best of our knowledge, this was the first study in which 3D displacements of fracture fragments have been evaluated for complex tibial plateau fractures. To build upon previous investigations regarding bi-condylar tibial plateau fractures, which only evaluated the facture fragment subsidences [23–31, 33, 45] or the frontal intra-articular gap movements [35], we presented a comprehensive 3D kinematic evaluation of all fracture fragments to illuminate the effects of coronal fracture lines.

During cyclic loading, the medial-anterior segment of Fracture C mainly moved in the longitudinal direction and exceeded 5-mm clinical failure which is indicative of a high risk for bone non-union. At the same time, the medial-posterior portion separated from the anterior one in the posterior direction with sagittal displacements exceeding 2 mm which indicates a risk of knee osteoarthritis (Fig. 8).

Due to the vertical nature of the coronal fracture line, the medial segments of Fracture C were subjected to higher shear forces [11]. Therefore, compared to Fracture H, the medial segments of Fracture C, especially medial-posterior one, demonstrated higher instability (Fig. 9). From sagittal rotational disparity between the two medial fragments, it can be concluded that coronal fracture line results in an articular step-off which may lead to knee osteoarthritis. Since sagittal rotations occurred due to screw bending, the coronal split mainly destabilized the anterior fragment perhaps due to the inclusion of fewer screws in comparison to its posterior counterpart. Regarding the frontal rotations, the contact between the load applicator and the coronal edges of the medial fragments in Fracture C resulted in reversing the movement of these fragments compared to Fracture H. For Fracture C in the 500-N cyclic load level, the diagonal screw which is the only connection between the medial fragments and mainly passes through the medial-posterior segment, lost its connection with the anterior one. Thus, medial-anterior fragment rotated in frontal direction, while the medial-posterior part remained stable. Importantly, longitudinal rotations demonstrate that the medial-posterior and medial-anterior fragments of Fracture C tilted away towards the posterior direction of the transverse plane. This separation resulted in higher loading on the medial-posterior part and consequently more longitudinal rotation compared to the medial-anterior one. It should be noted that for Fracture C there is a risk of malalignment in frontal and transverse planes due to exceeding the clinical failure criteria for sagittal and longitudinal rotations of the medial-anterior and medial-posterior fragments, respectively.

These biomechanical findings demonstrated that disregarding the coronal fracture line will result in overestimation of structural rigidity of tibial plateau fracture constructs. Also, the relative displacement of fracture fragments was considerably affected by the presence of a coronal split. While the medial fragment of Fracture H displaced mainly in the frontal plane, the coronal fracture resulted in rotational instabilities of both medial fragments. Therefore, with the presence of the coronal split, there is a risk of non-union at the tibial medial side as well as malalignment of the tibial plateau and eventually osteoarthrosis. With kinematic evaluations in mind, these consequences are likely to occur at lower load levels in Fracture C than in Fracture H. Noticeably due to higher relative rotations for the medial-posterior fragment and interfragmentary movements over 5 mm for medial anterior-shaft gap, an additional medial fixation could provide higher stability for Fracture C. These conclusions agree with previous clinical studies that have demonstrated higher clinical failure rates at the medial side of complex tibial plateau fractures [1, 2]. Also, it has been clinically [2, 11, 17, 19, 20] or biomechanically [45] observed that lateral locking implants may not adequately stabilize the posteromedial fragments of bi-condyla tibia plateau fractures and a supplementary medial implantation will be required.

Considering the clinically observed importance of posteromedial fragment for bi-condylar tibia plateau fractures, developing a biomechanical fracture model including the coronal fracture line is highly demanded [11]. Contrary to previous experimental studies, which applied loads only on the medial tibial plateau [23, 29, 32–34, 45], our load applicator was designed to simultaneously apply axial forces on both tibial plateau surfaces and distribute it 40% laterally and 60% medially, corresponding to physiological conditions [35, 36]. This load applicator with the adjustable position of the medial and lateral indenters can

be used even for cadaveric samples with various plateau widths. Moreover, using artificial femur condyles provided a more physiological contact pressure on the tibial plateau as compared to previous biomechanical studies [35]. Furthermore, like some of previous investigations [23, 26, 31], the fracture model of this study presented a highly unstable situation by removing the central triangle of bone from the proximal tibia. Comparing mechanical behaviors of the Horowitz fracture model among previous experimental studies [23, 26, 29, 31, 33, 35] is difficult due to some distinctions regarding sample types (composite or cadaveric bones), loading and boundary conditions as well as loading scenarios. In this regard, only the study of Lasanianos et al. [35] was almost similar to ours. The static stiffness of Fracture H was found to be 304 ± 95 N/mm which is in the same range of their reported value (400 ± 64 N/mm) [35]. The mentioned research group obtained higher static stiffness values for specimens fixed with lateral locking plates. A reason for this could be that the fracture model of their study was stiffer due to preserving the middle fracture gap. Also, a different distal boundary condition was assumed in their experimental setup. Failure load of Lasanianos et al.'s fracture model was almost three times that of Fracture H reported in the current research, since we assumed the clinical failure criteria which is in contrast with their mechanical failure criteria. Among previous biomechanical studies, only the investigation of Yoo et al. [45] considered a Horwitz fracture model consisting of the posteromedial fragment. However, their fracture model was different than our coronal fracture model developed based on the clinical review of Pätzold et al.'s study [1]. Fracture C includes a sagittal articular fracture line in addition to the proximal fracture gap that is located laterally compared to that of Yoo et al.'s fracture model. They reported failure load of the Sawbone samples fixed with the tibial less invasive stabilization system (LISS) to be 1680 ± 179 N that is almost 4.5 times that of Fracture C. This difference could be due to their stiff fracture model in which the middle fracture gap was preserved as well as the lateral articular split was not included. Additionally, they utilized a hemispherical impactor for exclusive loading on the medial tibial plateau, although our loading was performed with a dual applicator which simultaneously applies the axial force on both tibial plateaus. Moreover, their failure criteria were different than our clinical ones. Regarding the loading scenario, an incremental cyclic loading until failure was considered in this study. Unlike previous studies, in which the testing protocol did not include the incremental cyclic loading [23–35], the maximum load level of our gradual fatigue test increased stepwise by 50 N every 500 cycles. We believe that this progressive cyclic loading can simulate daily living activities of patients during the healing process, since after surgery incremental weight bearing on the injured limb is recommended.

Naturally, this study had some limitations which should be taken into consideration. First, artificial fourth-generation Sawbone samples were used for mechanical testing. Due to their material properties, their failure behavior might potentially differ from failure in human bone specimens. That is why we focused the failure analysis on relative movements between fragments rather than catastrophic failure of the fracture fixation construct. Also, Sawbone provided consistency in material, geometry, and mechanical properties, which increases the power to detect differences between groups. Second, the two fracture models were compared only under axial and bending loading conditions. The load applicator used in this study provided the sagittal rotational degree of freedom and consisted of femoral components of unilateral knee joint replacements which applied physiological pressure to the tibial plateau surface with distribution of 60% on the medial side and 40% laterally. In addition, the loading scenario only included axial knee joint forces, although for more realistic loading, the effect of muscle forces should also be considered. Moreover, instead of simulating the ankle joint, specimens were fixed distally to the testing machine directly, resulting in a somewhat overconstrained loading condition. Furthermore, to evaluate displacements and rotations, the fracture fragments were assumed as rigid parts. This assumption could be used due to high stiffness of the Sawbones which makes local deformations of segments negligible. Additionally, we simulated a hypothetical, unstable bi-condylar tibial plateau fracture in both fracture models by removing the central triangle of the proximal tibia as well as the side gap from the medial tibia. Last but not least, only one particular implant configuration with single lateral plating has been considered. With a more stable configuration like double medial and lateral platting which stabilizes the posterior fragment, the destabilizing effect of the coronal fracture is most likely less pronounced.

Conclusion

The outcomes of this study emphasize that it is mandatory for biomechanical simulations regarding complex tibial plateau fractures to be based on a clinically relevant fracture model such as ours (Fracture C) due to its ability to mimic native mechanical behavior more accurately than the traditional Horowitz model. The observed instability on the medial side of the coronal fracture model suggests that lateral plating alone provides insufficient mechanical fracture stabilization. We intend to pursue future research in this endeavor to propose the best fixation method for our novel fracture model.

Acknowledgements Open Access funding provided by Projekt DEAL. German Academic Exchange Service (DAAD), Bonn, Germany.

Author contributions All authors contributed to the study conception and design. Material preparation, data collection and analysis were performed by SS, RP, and MW. PA and SH also collaborated with others in data interpretation. The initial draft of the manuscript was written by SS, and all authors commented on that. The final manuscript was read and approved by all authors.

Funding There is no funding source.

Compliance with ethical standards

Conflict of interest The authors' research institution received institutional research support from Stryker Trauma, Selzach, Switzerland.

Ethical approval This article does not contain any studies with human participants or animals performed by any of the authors.

References

1. Pätzold R, Friederichs J, von Rüden C et al (2017) The pivotal role of the coronal fracture line for a new three-dimensional CT-based fracture classification of bicondylar proximal tibial fractures. Injury 48:2214–2220. https://doi.org/10.1016/j.injury.2017.06.019
2. Lee TC, Huang HT, Lin YC et al (2013) Bicondylar tibial plateau fracture treated by open reduction and fixation with unilateral locked plating. Kaohsiung J Med Sci 29:568–577. https://doi.org/10.1016/j.kjms.2013.01.006
3. Chang SM, Hu SJ, Zhang YQ et al (2014) A surgical protocol for bicondylar four-quadrant tibial plateau fractures. Int Orthop 38:2559–2564. https://doi.org/10.1007/s00264-014-2487-7
4. Menghi A, Mazzitelli G, Marzetti E et al (2017) Complex tibial plateau fractures: a retrospective study and proposal of treatment algorithm. Injury 48:S1–S6. https://doi.org/10.1016/S0020-1383(17)30649-6
5. Jiang R, Luo CF, Wang MC et al (2008) A comparative study of Less Invasive Stabilization System (LISS) fixation and two-incision double plating for the treatment of bicondylar tibial plateau fractures. Knee 15:139–143. https://doi.org/10.1016/j.knee.2007.12.001
6. Barei DP, Nork SE, Mills WJ et al (2004) Complications associated with internal fixation of high-energy bicondylar tibial plateau fractures utilizing a two-incision technique. J Orthop Trauma 18:649–657. https://doi.org/10.1097/00005131-200411000-00001
7. Barei DP, Nork SE, Mills WJ et al (2006) Functional outcomes of severe bicondylar tibial plateau fractures treated with dual incisions and medial and lateral plates. J Bone Jt Surg Am 88:1713–1721. https://doi.org/10.2106/JBJS.E.00907
8. Stevens DG, Beharry R, McKee MD et al (2001) The long-term functional outcome of operatively treated tibial plateau fractures. J Orthop Trauma 15:312–320. https://doi.org/10.1097/00005131-200106000-00002
9. Gosling T, Schandelmaier P, Muller M et al (2005) Single lateral locked screw plating of bicondylar tibial plateau fractures. Clin Orthop Relat Res 439:207–214. https://doi.org/10.1097/01.blo.0000176147.31756.4c
10. Partenheimer A, Gösling T, Müller M et al (2007) Management of bicondylar fractures of the tibial plateau with unilateral fixed-angle plate fixation. Unfallchirurg 110:675–683. https://doi.org/10.1007/s00113-007-1271-1
11. Barei DP, O'Mara TJ, Taitsman LA et al (2008) Frequency and fracture morphology of the posteromedial fragment in bicondylar tibial plateau fracture patterns. J Orthop Trauma 22:176–182. https://doi.org/10.1097/BOT.0b013e318169ef08
12. Hu YL, Ye FG, Ji AY et al (2009) Three-dimensional computed tomography imaging increases the reliability of classification systems for tibial plateau fractures. Injury 40:1282–1285. https://doi.org/10.1016/j.injury.2009.02.015
13. Krause M, Preiss A, Müller G et al (2016) Intra-articular tibial plateau fracture characteristics according to the "Ten segment classification". Injury 47:2551–2557. https://doi.org/10.1016/j.injury.2016.09.014
14. Hackl W, Riedl J, Reichkendler M et al (2001) Preoperative computerized tomography diagnosis of fractures of the tibial plateau. Unfallchirurg 104:519–523. https://doi.org/10.1007/s001130170115
15. Molenaars RJ, Mellema JJ, Doornberg JN, Kloen P (2015) Tibial plateau fracture characteristics: computed tomography mapping of lateral, medial, and bicondylar fractures. J Bone Jt Surg Am 97:1512–1520. https://doi.org/10.1097/bot.0000000000000511
16. Zeltser DW, Leopold SS (2013) Classifications in brief: schatzker classification of tibial plateau fractures. Clin Orthop Relat Res 471:371–374. https://doi.org/10.1007/s11999-012-2451-z
17. Weaver MJ, Harris MB, Strom AC et al (2012) Fracture pattern and fixation type related to loss of reduction in bicondylar tibial plateau fractures. Injury 43:864–869. https://doi.org/10.1016/j.injury.2011.10.035
18. von Rüden C, Samsami S, Pätzold R, Augat P (2018) Proximal tibial fractures: classifications and biomechanical principles—an update. Trauma und Berufskrankheit 20:230–236. https://doi.org/10.1007/s10039-018-0400-0
19. Kim CW, Lee CR, An KC et al (2016) Predictors of reduction loss in tibial plateau fracture surgery: focusing on posterior coronal fractures. Injury 47:1483–1487. https://doi.org/10.1016/j.injury.2016.04.029
20. Higgins TF, Kemper D, Klatt J (2009) Incidence and morphology of the posteromedial fragment in bicondylar tibial plateau fractures. J Orthop Trauma 23:45–51. https://doi.org/10.1097/BOT.0b013e31818f8dc1
21. Luo CF, Sun H, Zhang B, Zeng BF (2010) Three-column fixation for complex tibial plateau fractures. J Orthop Trauma 24:683–692. https://doi.org/10.1097/BOT.0b013e3181d436f3
22. Kfuri M, Schatzker J (2018) Revisiting the Schatzker classification of tibial plateau fractures. Injury 49:2252–2263. https://doi.org/10.1016/j.injury.2018.11.010
23. Horwitz DS, Bachus KN, Craig MA, Peters CL (1999) A biomechanical analysis of internal fixation of complex tibial plateau fractures. J Orthop Trauma 13:545–549
24. Wu CC, Tai CL (2007) Plating treatment for tibial plateau fractures: a biomechanical comparison of buttress and tension band

positions. Arch Orthop Trauma Surg 127:19–24. https://doi.org/10.1007/s00402-006-0192-8
25. Ali AM, Saleh M, Bolongaro S, Yang L (2006) Experimental model of tibial plateau fracture for biomechanical testing. J Biomech 39:1355–1360. https://doi.org/10.1016/j.jbiomech.2005.03.022
26. Mueller KL, Karunakar MA, Frankenburg EP, Scott DS (2003) Bicondylar tibial plateau fractures: a biomechanical study. Clin Orthop Relat Res 412:189–195. https://doi.org/10.1097/01.blo.0000071754.41516.e9
27. Ali AM, Yang L, Hashmi M, Saleh M (2001) Bicondylar tibial plateau fractures managed with the Sheffield Hybrid Fixator. biomechanical study and operative technique. Injury 32:SD86–91. https://doi.org/10.1016/s0020-1383(01)00165-6
28. Watson JT, Ripple S, Hoshaw SJ, Fyhrie D (2002) Hybrid external fixation for tibial plateau fractures: clinical and biomechanical correlation. Orthop Clin North Am 33:199–209. https://doi.org/10.1016/S0030-5898(03)00080-4
29. Egol KA, Su E, Tejwani NC et al (2004) Treatment of complex tibial plateau fractures using the less invasive stabilization system plate: clinical experience and a laboratory comparison with double plating. J Trauma 57:340–346. https://doi.org/10.1097/01.TA.0000112326.09272.13
30. Ali AM, Saleh M, Bolongaro S, Yang L (2003) The strength of different fixation techniques for bicondylar tibial plateau fractures: a biomechanical study. Clin Biomech (Bristol, Avon) 18:864–870. https://doi.org/10.1016/S0268-0033(03)00149-9
31. Higgins TF, Klatt J, Bachus KN (2007) Biomechanical analysis of bicondylar tibial plateau fixation: how does lateral locking plate fixation compare to dual plate fixation? J Orthop Trauma 21:301–306. https://doi.org/10.1097/BOT.0b013e3180500359
32. Lindeque B, Baldini T (2010) A biomechanical comparison of three different lateral tibia locking plates. Orthopedics 33:18–21. https://doi.org/10.3928/01477447-20091124-25
33. Gösling T, Schandelmaier P, Marti A et al (2004) Less invasive stabilization of complex tibial plateau fractures: a biomechanical evaluation of a unilateral locked screw plate and double plating. J Orthop Trauma 18:546–551. https://doi.org/10.1097/00005131-200409000-00011
34. Dougherty PJ, Kim DG, Meisterling S et al (2008) Biomechanical comparison of bicortical versus unicortical screw placement of proximal tibia locking plates: a cadaveric model. J Orthop Trauma 22:399–403. https://doi.org/10.1097/BOT.0b013e318178417e
35. Lasanianos NG, Garnavos C, Magnisalis E et al (2013) A comparative biomechanical study for complex tibial plateau fractures: nailing and compression bolts versus modern and traditional plating. Injury 44:1333–1339. https://doi.org/10.1016/j.injury.2013.03.013
36. Morrison JB (1970) The mechanics of the knee joint in relation to normal walking. J Biomech 3:51–61. https://doi.org/10.1016/0021-9290(70)90050-3
37. Ali AM, El-Shafie M, Willett KM (2002) Failure of fixation of tibial plateau fractures. J Orthop Trauma 16:323–329. https://doi.org/10.1097/00005131-200205000-00006
38. Holzach P, Matter P, Minter J (1994) Arthroscopically assisted treatment of lateral tibial plateau fractures in skiers: use of a cannulated reduction system. J Orthop Trauma 8:273–281
39. Doebele S, Siebenlist S, Vester H et al (2012) New method for detection of complex 3D fracture motion-verification of an optical motion analysis system for biomechanical studies. BMC Musculoskelet Disord 13:33. https://doi.org/10.1186/1471-2474-13-33
40. Kutzner I, Heinlein B, Graichen F et al (2010) Loading of the knee joint during activities of daily living measured in vivo in five subjects. J Biomech 43:2164–2173. https://doi.org/10.1016/j.jbiomech.2010.03.046
41. Bai B, Kummer FJ, Sala DA et al (2001) Effect of articular step-off and meniscectomy on joint alignment and contact pressures for fractures of the lateral tibial plateau. J Orthop Trauma 15:101–106. https://doi.org/10.1097/00005131-200102000-00005
42. Brown TD, Anderson DD, Nepola JV et al (1988) Contact stress aberrations following imprecise reduction of simple tibial plateau fractures. J Orthop Res 6:851–862. https://doi.org/10.1002/jor.1100060609
43. Tscherne HLP (1993) Tibial plateau fractures. Management and expected results. Clin Orthop Relat Res 292:87–100
44. Honkonen SE (1994) Indications for surgical treatment of tibial condyle fractures. Clin Orthop Relat Res 302:199–205
45. Yoo BJ, Beingessner DM, Barei DP (2010) Stabilization of the posteromedial fragment in bicondylar tibial plateau fractures: a mechanical comparison of locking and nonlocking single and dual plating methods. J Trauma Acute Care Surg 69:148–155. https://doi.org/10.1097/TA.0b013e3181e17060

8. Publication II

Medical Engineering and Physics 84 (2020) 84–95

Contents lists available at ScienceDirect

Medical Engineering and Physics

journal homepage: www.elsevier.com/locate/medengphy

Finite element analysis of Bi-condylar Tibial Plateau fractures to assess the effect of coronal splits

Shabnam Samsami[a,b,*], Sven Herrmann[b,d], Robert Pätzold[b,c], Martin Winkler[b], Peter Augat[b,d]

[a] Laboratory of Biomechanics and Experimental Orthopaedics, Department of Orthopedic Surgery, Physical Medicine and Rehabilitation, University Hospital of Munich (LMU), Fraunhoferstraße 20, 82152 Planegg, Munich, Germany
[b] Institute for Biomechanics, Berufsgenossenschaftliche Unfallklinik Murnau, Professor-Küntscher-Straße 8, 82418 Murnau, Germany
[c] Department of Trauma Surgery, Berufsgenossenschaftliche Unfallklinik, Professor-Küntscher-Straße 8, 82418 Murnau, Germany
[d] Institute for Biomechanics, Paracelsus Medical University, Strubergasse 21, 5020 Salzburg, Austria

ARTICLE INFO

Article history:
Received 6 February 2020
Revised 8 June 2020
Accepted 26 July 2020

Keywords:
Bi-condylar tibial plateau fracture
Coronal fracture line
Horwitz fracture model
Coronal fracture model
Finite element analysis
Validation
Stress distribution

ABSTRACT

Bi-condylar tibial plateau fractures are demanding to treat due to the complex geometry and the articular comminution. The presence of a coronal fracture line plays a crucial role in the fixation strategy. Disregarding this fracture line in previous biomechanical studies and established fracture classifications resulted in a lack of detailed knowledge regarding the influence of medial-posterior fragments on implant load sharings. This study aimed to evaluate the effects of coronal splits on stress distributions within the implants using the finite element analysis (FEA). FE models with (Fracture C) and without the coronal split (Fracture H) were developed and validated in order to assess stress distributions within the implant components. Comparing FE outcomes with biomechanical experiments indicated that both fracture models were well validated. FE evaluations demonstrated that the coronal split caused destabilization of the medial tibia, as well as a shift in the peak-stress areas from the middle part of the plate to the proximal section, and a 61% increase in the maximum stress of the kick-stand screw. Therefore, FE models based on clinically-relevant fracture morphologies can provide a reliable tool to assess implant failures as well as to compare different fracture fixation techniques.

1. Introduction

Bi-condylar tibial plateau fractures characterized by destabilization of both medial and lateral proximal condyles represent 35% of all tibial plateau fractures [1,2]. This fracture has the highest frequency in people between 40 and 60 years old and is more common in males than in females [1,2]. It occurs mainly as a result of varus or valgus stresses combined with axial loading [3]. Aims of an appropriate treatment include restoring knee joint functions and preventing osteoarthritis or limb mal-alignment [4]. Almost 50% of complex tibial plateau fractures present with a coronal fracture line which splits a posteromedial fragment [5–7]. Since fractures in the coronal plane are difficult to identify in bi-planar radiographs, preoperative 3D imaging is mandatory for adequate planning of the surgical treatment [4–6,8,9]. Presence of a coronal split often requires medial implants in addition to the lateral locking plate to stabilize the posteromedial fragment [6,10,11]. The established Schatzker and AO/OTA fracture classifications, however, have ignored this important fracture line [12].

Previous experimental studies on tibial plateau fractures have largely been based on the model developed by Horwitz et al. that emulates a Schatzker Type VI fracture [13–25]. Since this model is created according to a frontal projection of the fracture, it disregards coronal fracture lines as well as the presence of posteromedial fragments. Due to the inadequacy of this fracture model in reproducing complex fracture situations, the findings from these biomechanical studies have limited relevance for fractures with coronal splits and posteromedial fragments.

The finite element analysis (FEA) has proven to be an extremely useful tool for the development and correct applications of fracture fixation implants when simulations were properly verified and validated [26,27]. Verified and validated FE models can be analyzed regarding mechanical parameters such as strains or stresses, which are complicated, if not impossible, to measure in experi-

* Corresponding author.
E-mail addresses: biomechanik@bgu-murnau.de, shabnam.samsami@bgu-murnau.de (S. Samsami), Sven.Herrmann@bgu-murnau.de (S. Herrmann), Robert.Paetzold@bgu-murnau.de (R. Pätzold), winkler.riegsee@gmail.com (M. Winkler), Peter.Augat@bgu-murnau.de (P. Augat).

https://doi.org/10.1016/j.medengphy.2020.07.026
1350-4533/

ments [26,28]. Like biomechanical experiments, previous finite element studies for tibial plateau fractures have simulated neither complex fracture morphologies nor the presence of coronal splits [29–33].

Due to the lack of adequate models for the fixation of tibial plateau fractures, there is still a lack of understanding about the impact of the coronal fracture line on the load sharing within the bone-implant constructs. Such detailed knowledge would provide mechanical justification and educated evidence for implant selection. Therefore, this study used FEA to evaluate the effect of the coronal fracture line on the load distributions within fixation construct and fracture stability. To do so, FE models with and without a coronal fracture line were developed, validated, as well as compared with respect to stress distributions within the implants. We hypothesized that our coronal fracture model would exhibit higher stresses with distinct stress distributions within the implant compared to the traditional Horwitz model.

2. Material and methods

2.1. Study design

FEA was utilized to assess the effect of the fracture morphology on implant stress distributions by comparing two different fracture models simulated on synthetic tibia models fixed with the lateral locking plates: a traditional Horwitz fracture model (Fracture H) and a novel coronal fracture model (Fracture C). The FE models were validated with mechanical tests executed on synthetic samples under static single and semi-physiological loading conditions. Initially, the FE model of Fracture C was assessed with respect to simple single loading cases in five different force positions and in the axial direction. Then, the load case was extended to represent a semi-physiological loading scenario. The FE model of Fracture C was calibrated using both load cases, and afterwards the validity of FE simulations was assessed for the FE model of Fracture H. Subsequently, validated FE models were compared under semi-physiological loading regarding total deformations of bone-implant structures, load sharings between the medial and lateral tibial plateaus, as well as von-Mises stress distributions within the implant components.

2.2. Mechanical test to validate FEA of fracture models

2.2.1. Sample preparation

Fracture samples were prepared using two synthetic tibial bones (#3406 left large tibia, 4th Generation, Sawbones, Malmö, Sweden). The coronal fracture model (Fracture C) consisted of coronal and lateral articular splits identified in a systematic review of CT images [5]. In the superior view, the coronal fracture line divided the medial tibial plateau in two equal medial-anterior and medial-posterior segments. In the transverse plane, the sagittal fracture line separated the lateral plateau and intercondylar eminence of the tibia. Then, the lateral and medial osteotomies were performed from the Tuberculum intercondylare laterale to the lateral cortex at 4 cm and to the medial cortex at 6 cm distal from the tibial plateau, respectively. The medial and lateral ends were connected by a final cut, and the central segment was removed (Fig. 1). For Fracture H, the lateral and medial cortexes were cut from the intracondylar eminence to 4 cm from the lateral plateau and 6 cm from the medial plateau, respectively. The third cut from the lateral to the medial cortex removed the central bone gap (Fig. 1).

A board-certified orthopedic trauma surgeon fixed both fracture models using titanium locking plates (AxSOS Proximal Lateral Tibia Plate, left, six-hole length, Stryker, Selzach, Switzerland) and locking self-tapping screws of 4 mm diameters (four articular screws with 70 to 85 mm lengths, as well as six shaft screws with 20 to 32 mm lengths). A 3D-printed template was utilized to insert implants in both fracture models identically.

2.2.2. Experimental setup

The distal end of the tibia was embedded vertically in an aluminum box to a depth of 50 mm using a three-component casting resin (RenCast FC 53 A/B + Füller DT 082, Gößl + Pfaff GmbH, Karlskron/Brautlach, Germany). The box was fixed via a bench vise and a cross table to a testing machine (Zwick 010, Zwick GmbH & Co. KG, Germany) to provide the possibility for shifting the sample position from one loading point to another one in the single loading cases (Fig. 2.A). For semi-physiological loading, the embedding part was directly clamped to the base of an electro dynamic testing machine (Instron E3000, Instron Structural Testing, High Wycombe, United Kingdom) (Fig. 2.B).

Validation consisted of single and semi-physiological loading cases. In single loading, six static displacement-controlled ramps (10 mm/min) up to 350 N were applied at five different points (LA, LC, LP, MA, and MP) on the tibial plateau to cover a representative area for knee joint contact forces (Fig. 2.C) [34]. The first three static ramps of 75 N allowed the samples to settle, while the second three cycles up to 350 N were used to measure the stiffness of the tibia-implant constructs and local displacements. To remain within the linear elastic regions, the lateral positions (LA, LC, and LP) were loaded with 350 N, while the MA and MP positions were loaded with 75 N and 100 N, respectively. For instance, Fig. 2.A illustrates the experimental set-up for the LP position of this loading condition. The loads were introduced through a 10 mm-diameter steel ball attached to an aluminum cylinder. A horizontal linear slide connected the cylindrical indenter to the testing machine. The direction and position of the force were transferred to the FE models by virtually tracking the indenter of the testing machine.

For semi-physiological loading, the axial force was introduced through artificial femur condyles of unilateral knee replacements embedded in polyurethane blocks. These blocks were attached to the actuator of the testing machine with a hinge joint, which allowed the femur condyles to tilt in the frontal plane. To provide physiological load distribution with 60% loading on the medial tibial plateau [19,35], the distance of the femoral condyles was adjusted in such a way that the equidistant point and the axis of the testing machine were not aligned (Fig. 2.D). For this loading scenario, samples were subjected to six static displacement-controlled ramps (10 mm/min) up to 250 N which results in the elastic deformation. After settling of samples in the first three static ramps, the second three cycles were executed to determine global axial stiffness and local displacements. The location of the loading point was specified with an optical marker located on the center of the hinge joint in the frontal plane.

An optical measurement system (ARAMIS 5M, GOM GmbH, Braunschweig, Germany), with measurement error $< 0.1\%$ and 2%%for relative translational and rotational movements, respectively [36], was utilized to measure local displacements and axial deformation. Point markers and stochastic patterns were applied to the bone surfaces and the load applicator for visual tracking. For each fracture fragment, a set of 8 to 27 optical markers was considered, and coordinate data of markers were imported into ANSYS to calculate their displacements and to be compared with experimental data. The solid models of all fracture fragments and locking plates were virtually matched with the corresponding surface and point components by a best-fit algorithm included in GOM Correlate software (GOM Correlate Professional 2018, GOM GmbH, Braunschweig, Germany). Therefore, the position of the tibial shaft relative to the experimental coordinate system could be determined to provide the loading and boundary conditions for the

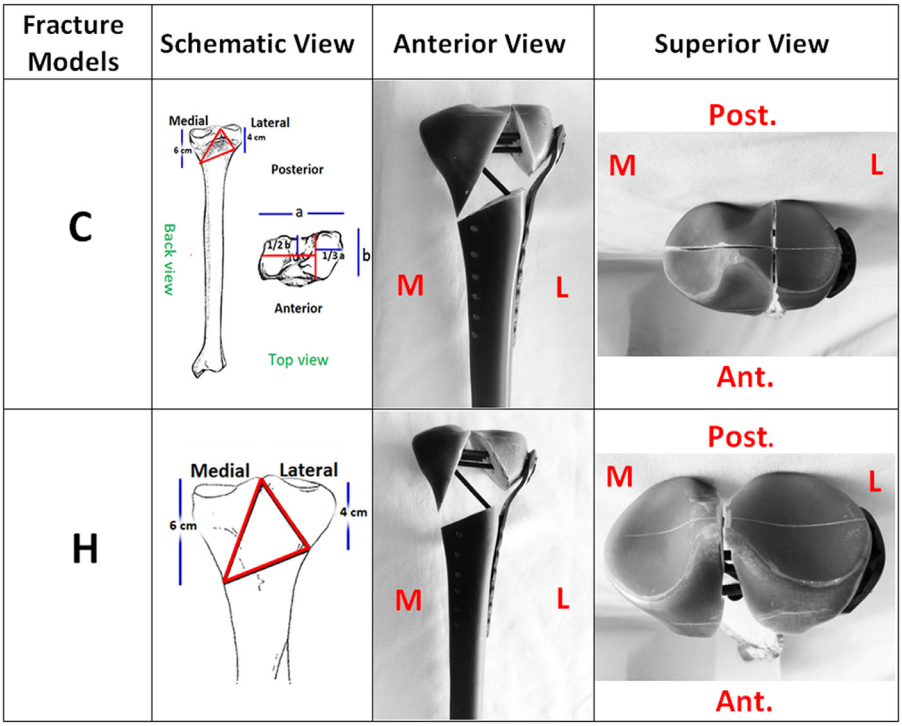

Fig. 1. Schematic drawings of Fractures C and H with anterior and superior views of prepared samples.

FE model. The loading coordinate systems were defined to evaluate the global axial displacement and stiffness (Fig. 2.A and B).

2.2.3. Experimental measurements

Axial stiffness and local marker displacements were experimentally evaluated to validate FE models. The axial stiffness was defined as the ratio of the applied load to the displacement of the load applicator in the axial direction.

2.3. Finite element analysis of fracture models

2.3.1. Geometry reconstruction

The geometry of FE models corresponded to the prepared samples for Fractures H and C. The CAD model of the intact tibia with a differentiation between cortical and cancellous bone was first generated from the CT data of the tibial Sawbone (SOMATOM Definition AS, Siemens Healthcare GmbH, Erlangen, Germany), with the following CT imaging parameters: peak voltage 120 kVp, tube current 106 mA, 0.75 mm slice thickness, pixel spacing 0.227\0.227 mm. Using AMIRA software (Visage Imaging GmbH, Berlin, Germany) the CT data were segmented to obtain a 3D reconstruction of the bone surface. Then, the segmented CT data were converted into a NURBS solid model with Geomagic Studio software (V.12, Geomagic, Morrisville, USA). The fracture models were simulated in computer-aided design (CAD) models of the intact tibia by slicing the aforementioned fracture lines for Fractures C and H. Then, the CAD model of the AxSOS proximal lateral tibia plate, provided by the company, was virtually implanted in both fracture models (Fig. 3.A). The highlighted holes and screws in Fig. 3.B demonstrate the maximum von-Mises stress areas which are explained in the discussion section. Screws were modeled as simple cylinders with 3.35 mm diameters corresponding to the inner diameter of the 4 mm locking screw and lengths as used in the experimental samples [37].

2.3.2. Spatial registration

Static FE models were computed in ANSYS® Workbench (ANSYS Academic Research, Release 19.3, ANSYS, Inc., Canonsburg, USA). By implementing a best-fit algorithm (GOM Correlate software), the position of the tibia bones relative to the testing machine as well as the initial positions of the load applicators and the distal clamps were spatially determined. Then, the required transfer matrices were calculated to corespond the spatial positions of the model components as well as the loading and boundary conditions between the FE models and experimental tests. The positions of the optical markers considered for validation of local displacements were also extracted from the GOM Correlate software and imported into ANSYS® Workbench [38,39].

2.3.3. Assigning material properties

The material properties for the synthetic tibia were assigned according to the manufacturer's specifications for the fourth-generation Sawbones (model 3406, Malmö, Sweden). The Young's modulus was set to 16.4 GPa and 155 MPa for the cortical and cancellous bone analogue, respectively, and a Poisson's ratio of 0.3 for both materials. For locking plates and screws, the material properties of TiAl6V4 with the Young's modulus of 110.4 GPa and the Poisson's ratio of 0.33 were employed. All materials were assumed to be homogeneous, isotropic, and linear elastic. For the embedding part and the distal aluminum cast, the Young modulus was set to 3.1 GPa and 700 GPa, respectively, and Poisson's ratios of 0.3. The semi-physiological load applicator was assumed as a rigid body.

2.3.4. Contact conditions

The FE model of Fracture C was designed with different contact types to determine which contact behavior was the most suitable to provide higher accuracy for numerical predictions, compared with experimental data (Table 1). After calibration of Fracture C in both load cases, the same contact assumptions were applied to Fracture H to evaluate the validity.

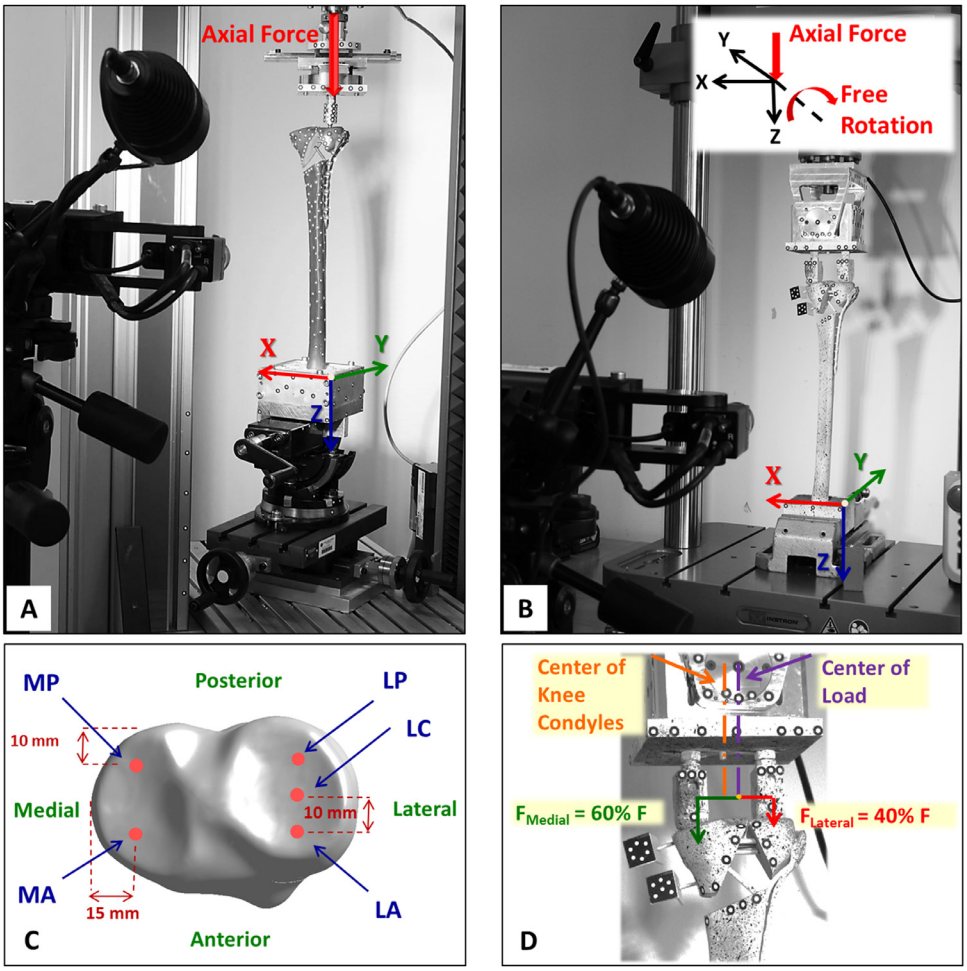

Fig. 2. Experimental set-up for validation of FE models in two loading conditions. (A) Single loading in which the picture shows the LP loading, and the force arrow was changed corresponding to each load position, (B) Semi-physiological loading, (C) Details of the single loading, in which the first letter of each label indicates the condyle and the second letter represents the location within the condyle: A = anterior, P = posterior, M = medial, L = lateral, C ==central, (D) Details of semi-physiological load applicator. In both experimental setups, the red vectors show the loading directions and degrees of freedom. The loading coordinate systems were also highlighted.

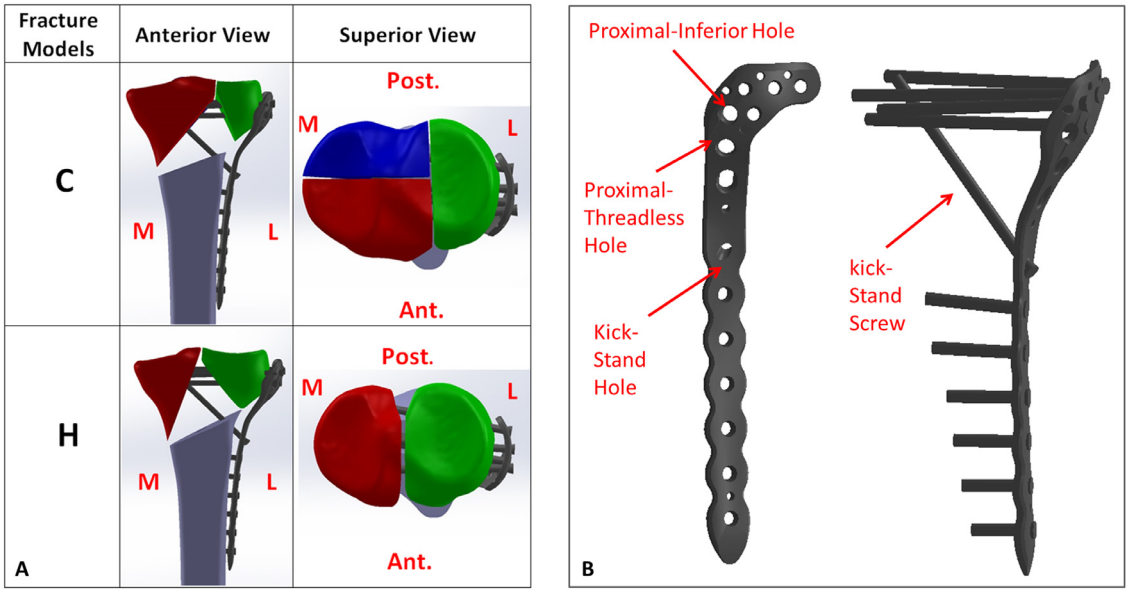

Fig. 3. (A) Solid models of Fractures C and H which were fixed with lateral locking plates and prepared for FEA, (B) Posterior and side views of the lateral locking implant in which the proximal-inferior, proximal-threadless, and kick-stand holes as well as the kick-stand screw are highlighted in order to refer to them in the discussion section regarding stress distributions within the implant.

Table 1
Contact details defined for each contact pairs in the FE models.

Contact Pair	Contact Type	Formulation	Detection Method	Normal Stiffness	Friction Coefficient	Interface Treatment
Screw-Plate	Bonded	MPC	Nodal: Normal from Target	-	-	-
Screw-Bone	Bonded	Pure Penalty	On Gauss Point	1	-	-
Kick-Stand Screw-Bone	Frictional	Pure Penalty	On Gauss Point	1	0.3	-
Embedding-Bone	Bonded	Pure Penalty	On Gauss Point	1	-	-
Embedding-Cast	Frictional	Augmented Lagrange	On Gauss Point	1	0.1	Adjust to Touch
Load Applicator-Bone	Frictionless	Augmented Lagrange	Nodal: Normal from Target	0.1	-	Adjust to Touch

By omitting screw threads, bone-screw interfaces were simulated as bonded contacts [37,40] with the normal stiffness factor of one. The reduced contact stiffness (instead of the default value of 10) allowed some numerical penetrations that could be more realistic assumptions for contacts between titanium screws and porous spongy bones [41]. In Fracture C, since the kick-stand screw was not completely located in the medial-anterior fragment, this bone-screw interface was assumed as a frictional type with a coefficient of 0.3, which has been previously used for titanium-spongy bone interfaces [42,43]. The interfaces between the locking screws and the plates were assumed as multi-point constraint contacts (MPC) which internally adds constraint equations to "tie" the displacements between contacting surfaces [41]. In the semi-physiological loading case, the interface between the tibial plateau and the load applicator was assumed to be frictionless because both tibial plateau and knee condyle surfaces were extremely smooth and polished. To simulate corner-surface contacts between the load applicator and the coronal split, the detection method of "normal direction from target surface" was selected [41]. For all interfaces, the contact stiffness was updated in each iteration to improve convergence behavior [44]. All contact areas were simulated as asymmetric pairs to efficiently establish all contact elements on one surface and all target elements on the corresponding surface [41].

2.3.5. Loading and boundary conditions

The validation step consisted of two single and semi-physiological loading cases. For both static scenarios, the directionsand magnitudes of the external forces, as well as boundary conditions were applied equivalent to experimental tests (Fig. 4). For each position of the single loading, a point force corresponding to the experimental condition was applied on the proximal tibial condyle (Fig. 4.A). In the semi-physiological loading scenario, the top surface of the load applicator was coupled to a remote point (loading center) that was able to freely rotate around the sagittal axis and translate along the vertical direction (Fig. 4.B).

2.3.6. Discretization of FE models

The solid models were meshed with 10-node tetrahedral elements including quadratic displacement functions. Convergence tests were executed to assess that a fine enough element discretization was used for FE analysis. For each part of fracture models (i.e. cortical and spongy bones, plate, screws, embedding material, and embedding cast), the element sizes were reduced until a convergence of the global axial displacement as well as the individual maximum von-Mises stresses for each specific part. In this regard, the node numbers of each part were increased by almost 30%, and if the numerical results of the global displacement and individual maximum von-Mises stress did not respectively change more than 3% and 5%%in three subsequent steps of sufficient mesh refinement, then the convergence element sizes were determined. A subsequent coarsening of the converged element size was carried out for all parts to check whether bigger element size can be selected for some parts if the changes in the global displacement and individual maximum von-Misses were less than 0.5% and 1%, respectively [39]. Bigger element sizes could be selected for the cortical and spongy parts of the distal tibial shaft (below the plate) because coarsening their element sizes had not significant effects on the numerical outcomes. Both FE models consisted of almost 845,000 Elements and 1,220,000 nodes.

2.3.7. Validation assessments

For each optical marker, the numerical local displacement was defined as the total displacement of the closest node to the location of the marker (Eq. 1) [38,39].

$$U_{tot} = \sqrt{u_x^2 + u_y^2 + u_z^2} \tag{1}$$

The overall axial stiffness was defined as the external axial load divided by the displacement of the load applicator projected in the loading direction. The global as well as local corroborations between FEA and the experiment were respectively assessed by regression analyses regarding the axial stiffness and the marker displacements as well as by root-mean-square errors (RSME) calculated for the marker displacements of each fracture fragment (Eq. 2), [38,42,45,46].

$$\mathrm{RMSE\%} = 100 * \sqrt{\frac{1}{n}\sum_{i=1}^{n}\left(\frac{\mathrm{FEA_i} - \mathrm{EXP_i}}{\mathrm{EXP_i}}\right)^2} \tag{2}$$

Moreover, the deviation of the numerical axial stiffness from the experimental measurements was evaluated in terms of percentage error to check the local accuracy of the FE models [43,44].

2.3.8. Outcomes of FE analyses

The global mechanical response of fracture models was assessed by analyzing the total displacement contours under semi-physiological loading. In addition, the medial and lateral contact reaction forces of the tibial plateaus were assessed to investigate the effect of the coronal split on the load shared between the tibial plateaus. Afterwards, von-Mises stress distributions within the lateral locking plates and screws were evaluated for both fracture models. Stress singularities due to sharp re-entrant corners or constraining points such as bonded contacts between locking screws and plates were ignored, and stress values were reported some nodes away from the local peak areas.

3. Results

3.1. FEA validation

Axial stiffness demonstrated a very strong agreement between numerical results and experimental measurements for Fracture C (R^2 = 99%; slope = 1.09, and intercept = -7.3 N/mm; Fig. 5.A) as well as for Fracture H (R^2 = 99%; slope = 0.99 and intercept = + 8.6 N/mm; Fig. 6.A). Although agreement for the marker displacement measurements was still strong, it was slightly smaller for Fracture H (R^2 = 87%; slope = 1.06 and intercept = -0.05 mm; Fig. 6.B) than that of Fracture C (R^2 = 96%; slope = 0.97 and intercept = -0.03 mm; Fig. 5.B). Root-mean-square errors of marker displacements and stiffness deviations were around 10% for Fracture C and about 10% larger for Fracture H (Table 2).

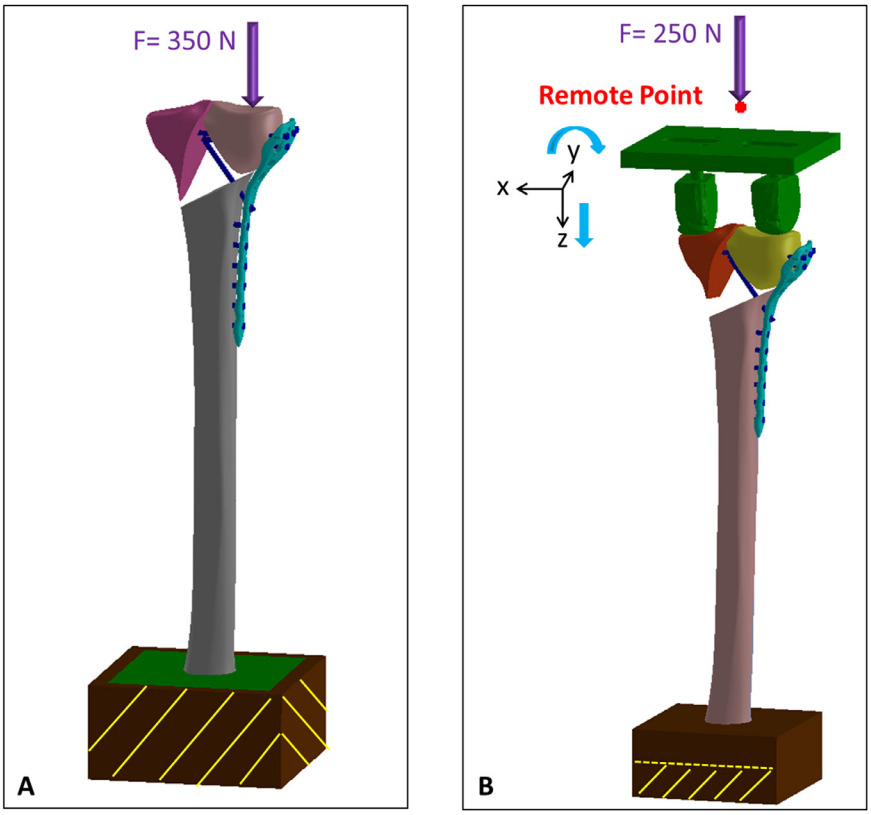

Fig. 4. Loading and boundary conditions applied in FE models for validation. (A) Single loading case in which as an example a 350 N point force applied on the LP position, and the force arrow was changed corresponding to each load position for four other loading points, (B) Semi physiological loading with the sagittal rotational and axial translational degrees of freedom.

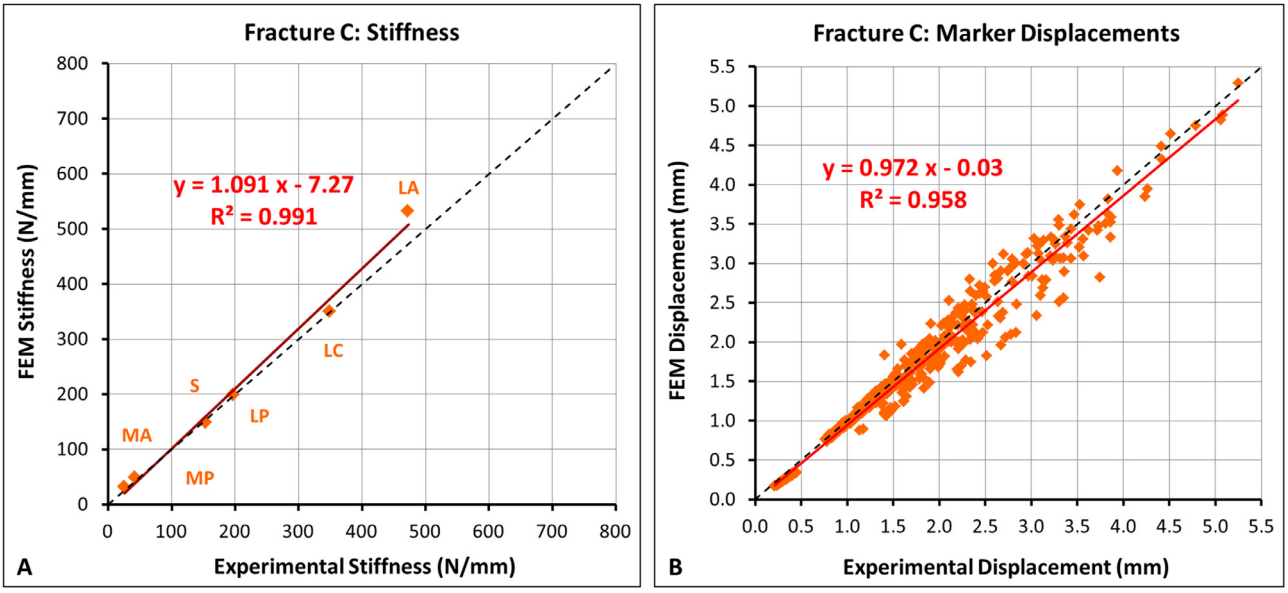

Fig. 5. Regression analysis of Fracture C. (A) Stiffness (LA, LC, LP, MA, and MP indicate single loading case and S indicates semi-physiological loading), (B) Local displacements.

Table 2
Accuracy of FEA for displacements and axial stiffness in single and semi-physiological loading scenarios.

Fracture	Loading	Lateral % RMSE	Medial % RMS		Shaft % RMSE	Stiffness % Error
			Anterior	**Posterior**		
C	**Single (Average)**	9.8	12.5	11.4	10.9	10.8
	Semi-Physiologic	7.9	7.1	7.5	3.7	-3.3
H	**Single (Average)**	18.4	19.8		21.8	14.2
	Semi-Physiologic	11.3	12.6		2.5	18.1

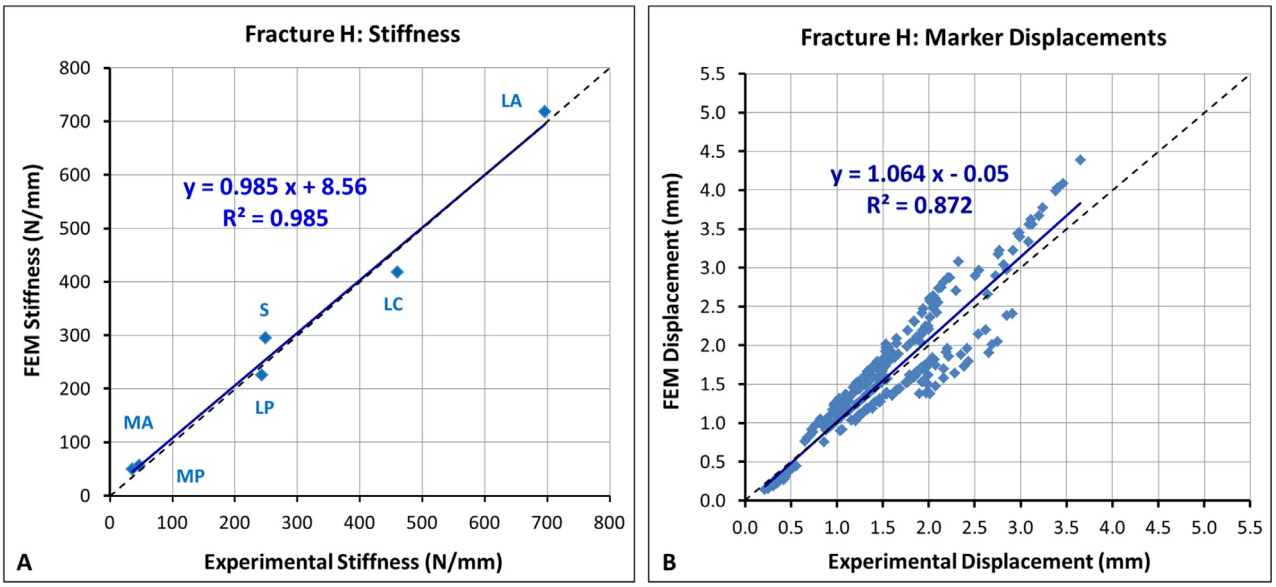

Fig. 6. Regression analysis of Fracture H. (A) Stiffness (LA, LC, LP, MA, and MP indicate single loading case and S indicates semi-physiological loading), (B) Local displacements.

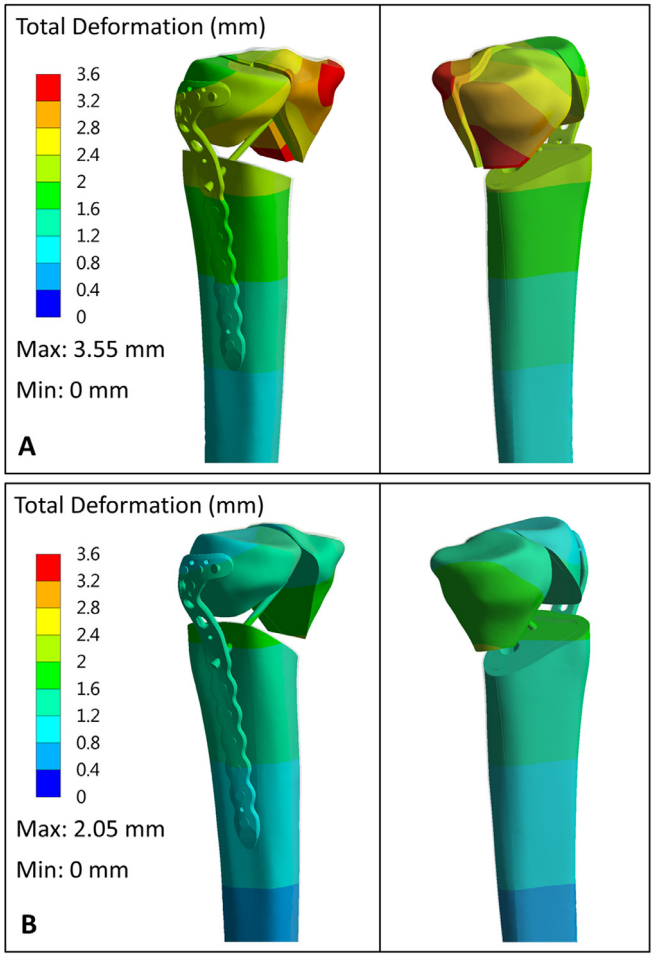

Fig. 7. Total deformation of tibia-implant structures for both FE models. (A) Fracture C, (B) Fracture H.

3.2. Evaluation of total deformations and stress distributions

FE analysis of total deformations indicated that Fracture C showed 73% higher overall deformation, compared to Fracture H. The coronal fracture line resulted in instability which rotated the medial-anterior fragment in the frontal plane and tilted away its posterior counterpart in the transverse plane. The medial section of Fracture H, however, is mainly displaced in the frontal plane (Fig. 7).

The effect of fracture morphology on the load shared between the medial and lateral sides of the tibia was also interesting. In Fracture H, the external load was shared almost equally on both tibial sides (56% on the lateral and 44% on the medial tibial plateau), while the lateral fragment of Fracture C carried 61% of the axial external load as well as the medial-anterior and medial-posterior fragments transferred 23% and 16% of this force, respectively.

Von-Mises stress contours of the inner surfaces of the plates indicated that for Fracture C, the peak stress, which occurred around the proximal-inferior and proximal-threadless holes, was almost 70% higher than that of Fracture H, which was observed around the kick-stand hole. At the outer surfaces of the plate, Fracture C demonstrated an almost 62% higher peak stress, compared to that of Fracture H. The high-stress areas at the outer surface of the plate were mainly in the vicinity of the proximal-threadless hole for fracture C and around the kick-stand hole in Fracture H. Therefore, in Fracture C, the main load is transferred through the proximal part of the lateral locking plate, while for Fracture H, the middle section of the plate is the main load-bearing part (Fig. 3.B and Fig. 8).

Comparing von-Mises stress distributions in screws, Fracture C revealed a 61% higher maximum stress than that of Fracture H. For both, the peak stress areas were found in the inferior surface (compression side) of the kick-stand screws which is in contact with cortical tibial bone (Fig. 9 and Fig. 10). In Fracture C, the kick-stand and proximal-dorsal screws were highly loaded and showed maximum stress areas with values of 427 MPa and 325 MPa, respectively. For the proximal-inferior screw, only a small area around the screw head, which was bonded to the plate, demonstrated a stress-concentration of 123 MPa, and the rest of the screw shafts had only minor stress values. Moreover, the proximal-middle screw did not play a role in load sharing (Fig. 9). Contrastingly, for Fracture H, the kick-stand screw carried the highest loads with 265 MPa maximum stress, while the proximal-dorsal and proximal-inferior screws demonstrated 115 and 60 MPa von-Mises stress values, re-

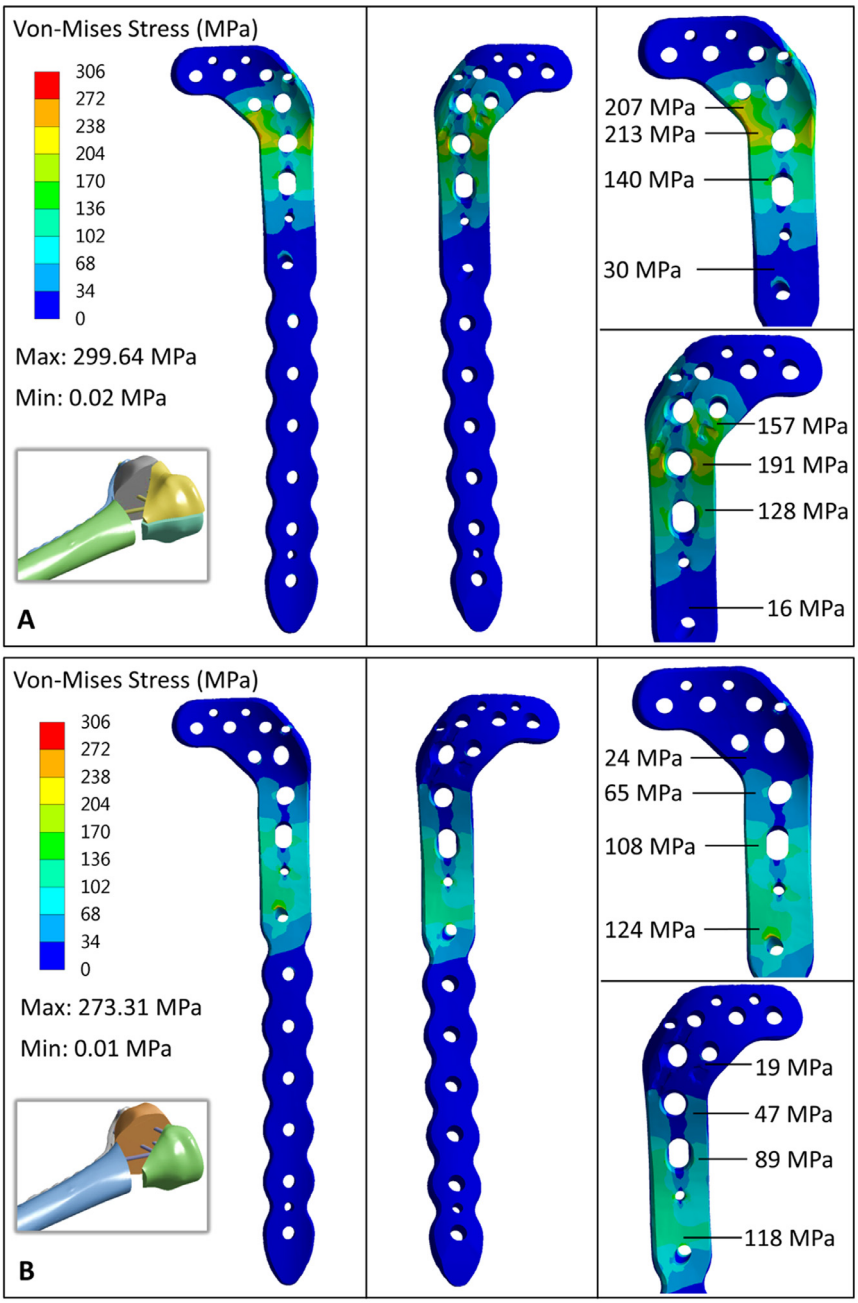

Fig. 8. Von-Mises stress distributions for the inner and outer surfaces of the lateral locking plates in the fracture FE models. (A) Fracture C, (B) Fracture H.

spectively. Additionally, among proximal screws, the anterior one indicated a minimum stress (Fig. 10).

4. Discussion

The crucial role of the posteromedial fragment for the fixation of bi-condylar tibial plateau fractures has been clinically well recognized [6,10,11]. In contrast, there is a lack of understanding regarding the biomechanical consequences of this fracture instability. Therefore, the aim of this study was to evaluate the effect of the coronal split on fracture stability and stress distribution within the implants. Using validated numerical models, our findings indicated that the coronal split destabilizes the medial side of the fracture, leading to decreased fracture stiffness and to increased total fragment deformation. In particular, the relative displacements of the medial fragments with respect to the tibial shaft were larger in Fracture C, compared with Fracture H. Analysis of the stress distributions within the implant components demonstrated that the coronal fracture line shifted the high-stress areas from the middle section of the lateral locking plate to the proximal part. Also, the peak stress observed at the kick-stand screw as the main load-bearing screw was drastically increased.

Numerical simulations are reliable if their outcomes are appropriately justified by verification and validation [27,46,47]. Inspired by previous studies [38,39,42–45,48,49], the mandatory steps for FE verification as well as validation were executed for our FE models. In both loading cases, FEA of both fractures revealed acceptable accuracies, while the FE model of Fracture C demonstrated superior agreement with experimental outcomes than that of Fracture H. Applying different assumptions for the interface between the medial fragment and the kick-stand screw in fracures C and

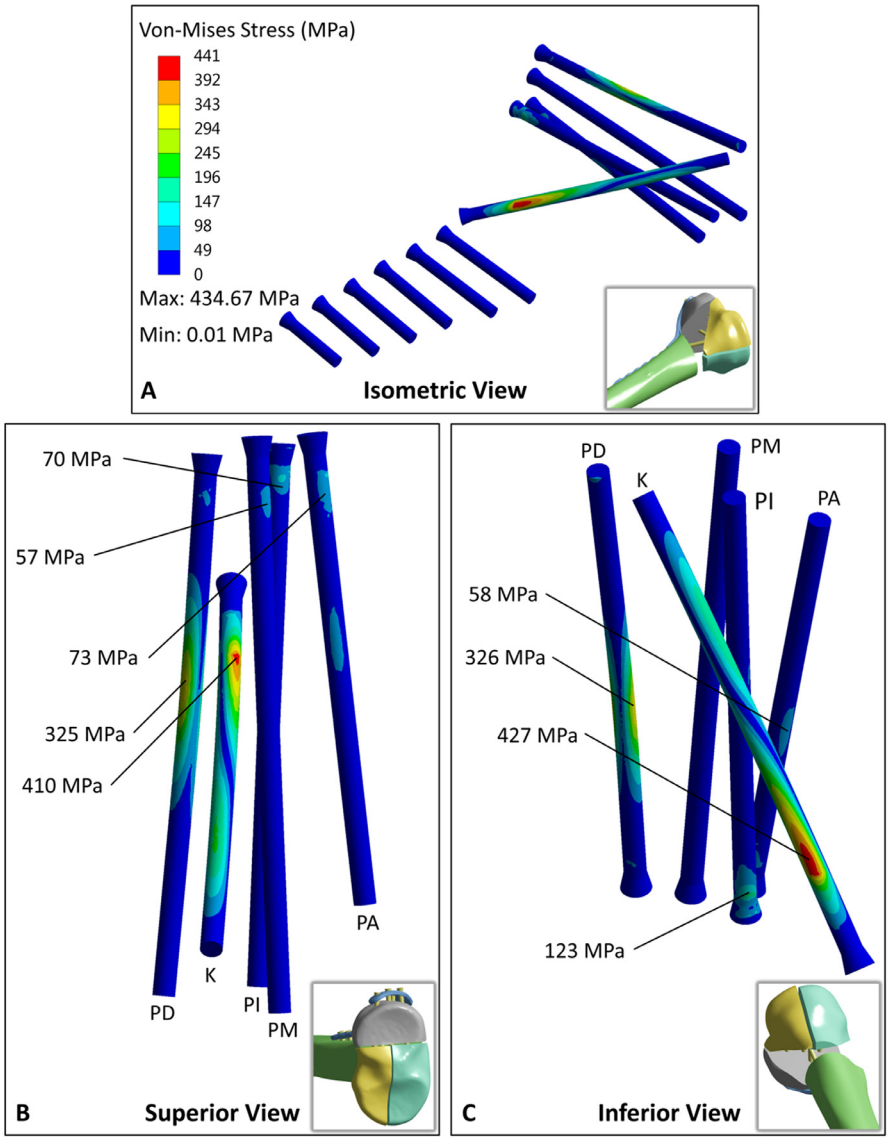

Fig. 9. Different views of von-Mises stress distributions for locking screws of Fracture C. (A) Isometric, (B) Superior, (C) Inferior views.

H is supposed to be the main reason regarding larger errors for the FE model of Fracture H than Fracture C's. The kick-stand screw was fully integrated into Fracture H with the bonded contact, while according to experimental observations for Fracture C, its interface with the medial-anterior segment should be modeled as a frictional contact. Accordingly, the FE outcomes of Fracture H are more sensitive to the location of the loading position with respect to this screw, and our unpublished sensitivity analysis also confirmed that. Furthermore, in semi-physiological loading condition, the higher structural rigidity of Fracture H resulted in displacement values below 1 mm, and a slight deviation between numerical and experimental outcomes introduced larger relative inaccuracy. In Fracture C, the regression curve of marker displacements demonstrated some data deviations. It could be related to different tracking method for the medial-posterior fragment that was located out of camera views or some errors in the plate position.

Some previous studies conducted FE analysis regarding tibial plateau fractures, but none of them were validated against experimental data [29,30,32,33,36]. More importantly, similar to previous experimental investigations [13–25], these studies also disregarded complex morphologies of bi-condylar fractures consisting of coronal splits. According to the obtained results for semi-physiological loading, the static stiffness of Fracture H was 295 N/mm which is in the same range of experimental values reported by Lasanianos et al. (400 ± 64 N/mm) [19]. The difference between these values could be due to the preservation of the bone fracture gaps or distinctions in experimental boundary conditions.

The total deformation of bone-implant structures revealed that the presence of the coronal fracture line destabilized the medial side of the tibia which was inadequately fixed with single lateral plating only. This outcome is in agreement with previous clinical studies indicating that the clinical failures of complex tibial plateau fractures mainly occurrs at the medial side [5,50], as well as noting that double plating is required for bi-condylar tibia plateau fractures with coronal splits [2,6,51,52].

The numerical evaluations of the axial reaction forces on the tibia plateaus illustrated that since the lateral side of Fracture C was stiffer than its medial counterpart, the lateral tibia plateau transferred 61% of the external load. Previous FE studies regarding tibial plateau or proximal tibial fractures, however, mainly applied the knee contact forces as simple pressures on the tibial plateau with 60% distribution on the medial side [29,31,33,53,54]. Although

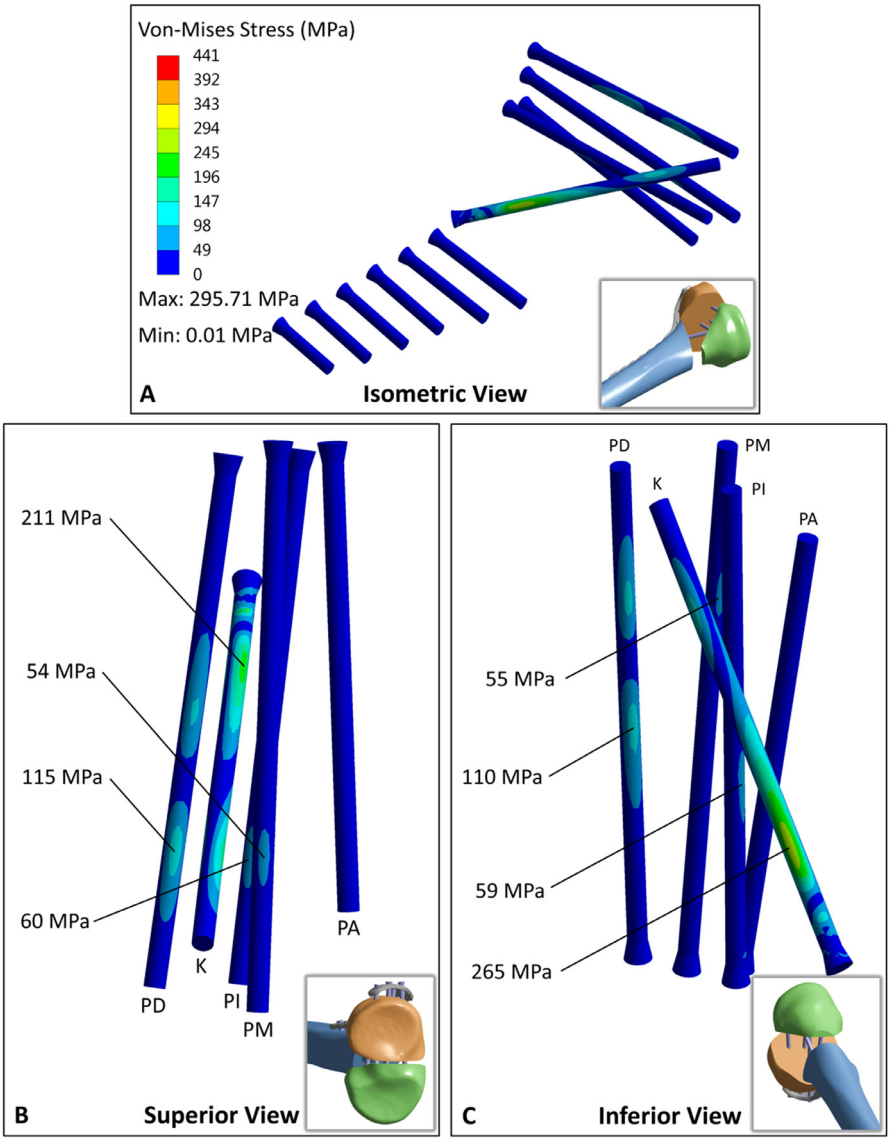

Fig. 10. Different views of von-Mises stress distributions for locking screws of Fracture H. (A) Isometric, (B) Superior, C) Inferior view.

60% of the knee contact force is transferred through the medial plateau of the intact tibia [35,55], the current FE simulations and our pilot mechanical tests demonstrated that for the tibia-implant structures, the load sharing between the medial and lateral sides depended on their relative rigidity. Therefore, our designed load applicator in addition to providing more realistic contact areas on the tibial plateau surface distributed the external loads corresponding to the relative rigidity of the tibial plateaus, which most likely represent clinical reality.

Our results regarding implant stress distributions are helpful in improving plate designs or fixation methods for this complex fracture. The locations of maximum von-Mises stresses are the potential failure points in cases of repetitive loading. All peak stress values were smaller than the yield strength of Ti6Al4V (800 MPa) [30]. In both fracture models, the maximum von-Mises stress of the kick-stand screw was almost twice that of the plate. Thus, it can be predicted that the screw fatigue failure would occur sooner than the plate failure. Due to the coronal split, the medial side of Fracture C was laxer than Fracture H's. That is why the lateral side of Fracture C was subjected to almost 11% more load which caused higher von-Mises stress values in the lateral locking plate and screws.

Stress distribution contours indicated that the coronal fracture line resulted in altering the potential failure points of the lateral locking plate from the middle section (in Fracture H) to the proximal part (in Fracture C) as well as remarkably increasing the peak von-Mises stress of the kick-stand screw. In Fracture C, the kick-stand and proximal-dorsal screws were the main load-bearing screws, while in Fracture H, the load was mostly transferred by the kick-stand screw. Therefore, disregarding this crucial fracture line leads to distinct predictions about the failure sites of the lateral locking plate under fatigue loading or the failure loads of the kick-stand screw.

According to the obtained values for maximum von-Mises stresses of the lateral locking implantation in Fracture C, in the case of full-weight bearing, in which peak of knee contact forces increased to almost three times of the body-weight, approximately 2500 N [56], the kick-stand screw or the proximal section of the lateral locking plate would be plastically deformed. This outcome is also in alignment with previous clinical studies which empha-

sized on insufficiency of single lateral platting for complex tibial plateau fractures including the posteromedial fragments [6,51,52].

This study also had some limitations which should be mentioned. First, although our models were validated in terms of axial stiffness and marker displacements, stress contours of the implant components were not verified. Nevertheless, we assume that stress calculations in the metallic components to be reliable. Its supporting reason is that the applied loads did not result in plastic deformations or screw loosening. Also, displacements and stiffness which both primarily result from implant deformation were very accurately predicted, providing sufficient trust in the numerical model. As another limitation, due to FE simplifications regarding the bone-screw and the screw-plate interfaces, the mentioned stress results were just estimations to assess the effects of fracture morphology. However, it is expected that the real patterns of stress contours for the plate and the screw shank would remain about the same. In addition, the FE models were based on Sawbones instead of human bones. It has been shown that mechanical properties of the fourth-generation Sawbones are very close to cadaveric bones. Since the geometry and the mechanical properties of synthetic bones are constant [57,58], they were suitable for our study. Furthermore, the FE models were validated only under axial and bending loading conditions, since in all activities the axial component of the knee contact forces is dominant [56]. Moreover, muscle forces were not regarded in FE simulations, and only the knee contact force was considered for loading conditions. Finally, distal boundary conditions were simplified with embedding cubes instead of simulating the ankle joint.

5. Conclusion

In conclusion, outcomes of this study reveal that the coronal splits of complex tibial plateau fractures remarkably affect the stress distributions within locking implants in addition to destabilizing the medial side of the tibia. Therefore, the potential fatigue failure points of lateral locking plates and screws depend on the fracture morphology, and a clinically-relevant fracture model such as Fracture C should be considered to accurately assess fixation methods. The presented validated FE model of bi-condylar tibial plateau fractures including coronal splits provides the potential to assess the effects of implant designs, plate positions, and screw orientations on the fixation stability of these clinically-challenging fractures.

Declaration of Competing Interest

The authors' research institution received institutional research support by Stryker Company, Selzach, Switzerland.

Funding

None.

Ethical approval

Not required.

Acknowledgements

German Academic Exchange Service (DAAD), Bonn, Germany.

References

[1] Elsoe R, Larsen P, Nielsen NPH, Swenne J, Rasmussen S, Ostgaard SE. Population-based epidemiology of tibial plateau fractures. Orthopedics 2015;38:e780–6. https://doi.org/10.3928/01477447-20150902-55.

[2] Pätzold R, Spiegl U, Wurster M, Augat P, Gutsfeld P, Gonschorek O, et al. [Proximal tibial fractures sustained during alpine skiing - Incidence and risk factors]. Sportverletzung-Sportschaden 2013;27:207–11. https://doi.org/10.1055/s-0033-1356108.

[3] Markhardt BK, Gross JM, Monu JUV. Schatzker classification of tibial plateau fractures: Use of CT and MR imaging improves assessment. Radiographics 2009;29:585–97. https://doi.org/10.1148/rg.292085078.

[4] Krause M, Preiss A, Müller G, Madert J, Fehske K, Neumann M V, et al. Intra-articular tibial plateau fracture characteristics according to the "Ten segment classification". Injury 2016;47:2551–7. https://doi.org/10.1016/j.injury.2016.09.014.

[5] Pätzold R, Friederichs J, von Rüden C, Panzer S, Bühren V, Augat P. The pivotal role of the coronal fracture line for a new three-dimensional CT-based fracture classification of bicondylar proximal tibial fractures. Injury 2017;48:2214–20. https://doi.org/10.1016/j.injury.2017.06.019.

[6] Barei DP, O'Mara TJ, Taitsman LA, Dunbar RP, Nork SE. Frequency and fracture morphology of the posteromedial fragment in bicondylar tibial plateau fracture patterns. J Orthop Trauma 2008;22:176–82. https://doi.org/10.1097/BOT.0b013e318169ef08.

[7] Weaver MJ, Harris MB, Strom AC, Smith RM, Lhowe D, Zurakowski D, et al. Fracture pattern and fixation type related to loss of reduction in bicondylar tibial plateau fractures. Injury 2012;43:864–9. https://doi.org/10.1016/j.injury.2011.10.035.

[8] Hu YL, Ye FG, Ji AY, Qiao GX, Liu HF. Three-dimensional computed tomography imaging increases the reliability of classification systems for tibial plateau fractures. Injury 2009;40:1282–5. https://doi.org/10.1016/j.injury.2009.02.015.

[9] Hackl W, Riedl J, Reichkendler M, Benedetto KP, Freund M, Bale R. [Preoperative computerized tomography diagnosis of fractures of the tibial plateau]. Unfallchirurg 2001;104:519–23. https://doi.org/10.1007/s001130170115.

[10] Jiang R, Luo CF, Wang MC, Yang TY, Zeng BF. A comparative study of Less Invasive Stabilization System (LISS) fixation and two-incision double plating for the treatment of bicondylar tibial plateau fractures. Knee 2008;15:139–43. https://doi.org/10.1016/j.knee.2007.12.001.

[11] Barei DP, Nork SE, Mills WJ, Henley MB, Benirschke SK. Complications associated with internal fixation of high-energy bicondylar tibial plateau fractures utilizing a two-incision technique. J Orthop Trauma 2004;18:649–57. https://doi.org/10.1097/00005131-200411000-00001.

[12] Molenaars RJ, Mellema JJ, Doornberg JN, Kloen P. Tibial plateau fracture characteristics: computed tomography mapping of lateral, medial, and bicondylar fractures. J Bone Jt Surg Am 2015;97:1512–20. https://doi.org/10.1097/bot.0000000000000511.

[13] Horwitz DS, Bachus KN, Craig MA, Peters CL. A biomechanical analysis of internal fixation of complex tibial plateau fractures. J Orthop Trauma 1999;13:545–9. https://doi.org/10.1097/00005131-199911000-00005.

[14] Ali AM, Saleh M, Bolongaro S, Yang L. The strength of different fixation techniques for bicondylar tibial plateau fractures – a biomechanical study. Clin Biomech 2003;18:864–70. https://doi.org/10.1016/S0268-0033(03)00149-9.

[15] Lindeque B, Baldini T. A biomechanical comparison of three different lateral tibia locking plates. Orthopedics 2010;33:18–21. https://doi.org/10.3928/01477447-20091124-25.

[16] Wu CC, Tai CL. Plating treatment for tibial plateau fractures: a biomechanical comparison of buttress and tension band positions. Arch Orthop Trauma Surg 2007;127:19–24. https://doi.org/10.1007/s00402-006-0192-8.

[17] Gösling T, Schandelmaier P, Marti A, Hufner T, Partenheimer A, Krettek C. Less invasive stabilization of complex tibial plateau fractures: a biomechanical evaluation of a unilateral locked screw plate and double plating. J Orthop Trauma 2004;18:546–51. https://doi.org/10.1097/00005131-200409000-00011.

[18] Dougherty PJ, Kim DG, Meisterling S, Wybo C, Yeni Y. Biomechanical comparison of bicortical versus unicortical screw placement of proximal tibia locking plates: a cadaveric model. J Orthop Trauma 2008;22:399–403. https://doi.org/10.1097/BOT.0b013e318178417e.

[19] Lasanianos NG, Garnavos C, Magnisalis E, Kourkoulis S, Babis GC. A comparative biomechanical study for complex tibial plateau fractures: nailing and compression bolts versus modern and traditional plating. Injury 2013;44:1333–9. https://doi.org/10.1016/j.injury.2013.03.013.

[20] Ali AM, Saleh M, Bolongaro S, Yang L. Experimental model of tibial plateau fracture for biomechanical testing. J Biomech 2006;39:1355–60. https://doi.org/10.1016/j.jbiomech.2005.03.022.

[21] Mueller KL, Karunakar MA, Frankenburg EP, Scott DS. Bicondylar tibial plateau fractures: a biomechanical study. Clin Orthop Relat Res 2003;412:189–95. https://doi.org/10.1097/01.blo.0000071754.41516.e9.

[22] Ali AM, Yang L, Hashmi M, Saleh M. Bicondylar Tibial plateau fractures managed with the Sheffield Hybrid fixator. Biomech Study Oper. Tech. Inj. 2001;32:SD86–91. https://doi.org/10.1016/s0020-1383(01)00165-6.

[23] Watson JT, Ripple S, Hoshaw SJ, Fyhrie D. Hybrid external fixation for tibial plateau fractures: clinical and biomechanical correlation. Orthop Clin North Am 2002;33:199–209. https://doi.org/10.1016/S0030-5898(03)00080-4.

[24] Egol KA, Su E, Tejwani NC, Sims SH, Kummer FJ, Koval KJ. Treatment of complex tibial plateau fractures using the less invasive stabilization system plate: clinical experience and a laboratory comparison with double plating. J Trauma 2004;57:340–6. https://doi.org/10.1097/01.TA.0000112326.09272.13.

[25] Higgins TF, Klatt J, Bachus KN. Biomechanical analysis of bicondylar tibial plateau fixation: How does lateral locking plate fixation compare to dual plate fixation? J Orthop Trauma 2007;21:301–6. https://doi.org/10.1097/BOT.0b013e3180500359.

[26] Kluess D. Finite element analysis in orthopaedic biomechanics. In: Moratal D, editor. Finite element analysis. Intech Open; 2010. p. 151–71.
[27] Yosibash Z. Principles of Finite Elements Analysis. In: Simpson H, Augat P, editors. Experimetal research methods in Orthopedic and trauma. Stuttgart, New York, Delhi: Rio: Thieme Publishing Group; 2015. p. 145–55.
[28] Kluess D, Souffrant R, Mittelmeier W, Wree A, Schmitz KP, Bader R. A convenient approach for finite-element-analyses of orthopaedic implants in bone contact: modeling and experimental validation. Comput Methods Programs Biomed 2009;95:23–30. https://doi.org/10.1016/j.cmpb.2009.01.004.
[29] Huang X, Zhi Z, Yu B, Chen F. Stress and stability of plate-screw fixation and screw fixation in the treatment of Schatzker type IV medial tibial plateau fracture: a comparative finite element study. J Orthop Surg Res 2015;10:1–9. https://doi.org/10.1186/s13018-015-0325-2.
[30] Carrera I, Gelber PE, Chary G, González-Ballester MA, Monllau JC, Noailly J. Fixation of a split fracture of the lateral tibial plateau with a locking screw plate instead of cannulated screws would allow early weight bearing: a computational exploration. Int Orthop 2016;40:2163–9. https://doi.org/10.1007/s00264-015-3106-y.
[31] Chen P, Lu H, Shen H, Wang W, Ni B, Chen J. Newly designed anterolateral and posterolateral locking anatomic plates for lateral tibial plateau fractures: a finite element study. J Orthop Surg Res 2017;12:1–9. https://doi.org/10.1186/s13018-017-0531-1.
[32] Belaid D, Germaneau A, Bouchoucha A, Brémand F, Brèque C, Rigoard P, et al. Finite element analysis of mechanical behavior of stabilization techniques for tibial plateau fractures. Comput Methods Biomech Biomed Engin 2017;20:13–14. https://doi.org/10.1080/10255842.2017.1382837.
[33] Chen F, Wu S, Zhong Z, Huang X, Ao R, Zhang X, et al. Stress and stability of newly designed medial anatomic locking plates and traditional fixations in the treatment of posterointernal tibial plateau fracture: a comparative finite element study. Int J Clin Exp Med 2018;11:12956–63.
[34] Gray HA, Zavatsky AB, Taddei F, Cristofolini L, Gill HS. Experimental validation of a finite element model of a composite tibia. Proc Inst Mech Eng H 2007;221:315–24. https://doi.org/10.1243/09544119JEIM119.
[35] Morrison JB. The mechanics of the knee joint in relation to normal walking. J Biomech 1970;3:51–61. https://doi.org/10.1016/0021-9290(70)90050-3.
[36] Doebele S, Siebenlist S, Vester H, Wolf P, Hagn U, Schreiber U, et al. New method for detection of complex 3D fracture motion – verification of an optical motion analysis system for biomechanical studies. BMC Musculoskelet Disord 2012;13:33. https://doi.org/10.1186/1471-2474-13-33.
[37] Inzana JA, Varga P, Windolf M. Implicit modeling of screw threads for efficient finite element analysis of complex bone-implant systems. J Biomech 2016;49:1836–44. https://doi.org/10.1016/j.jbiomech.2016.04.021.
[38] Trabelsi N, Yosibash Z, Wutte C, Augat P, Eberle S. Patient-specific finite element analysis of the human femur- a double-blinded biomechanical validation. J Biomech 2011;44:1666–72. https://doi.org/10.1016/j.jbiomech.2011.03.024.
[39] Eberle S, Göttlinger M, Augat P. An investigation to determine if a single validated density-elasticity relationship can be used for subject specific finite element analyses of human long bones. Med Eng Phys 2013;35:875–83. https://doi.org/10.1016/j.medengphy.2012.08.022.
[40] MacLeod AR, Pankaj P, Simpson AH. Does screw-bone interface modelling matter in finite element analyses? J Biomech 2012;45:1712–16. https://doi.org/10.1016/j.jbiomech.2012.04.008.
[41] ANSYS Academic Research Workbench, Release 19.3, Help system, Contact technology guide, ANSYS, Inc. https://ansyshelp.ansys.com.
[42] Eberle S, Gerber C, Von Oldenburg G, Högel F, Augat P. A biomechanical evaluation of orthopaedic implants for hip fractures by finite element analysis and in-vitro tests. Proc Inst Mech Eng H 2010;224:1141–52. https://doi.org/10.1243/09544119JEIM799.
[43] Henschel J, Eberle S, Augat P. Load distribution between cephalic screws in a dual lag screw trochanteric nail. J Orthop Surg Res 2016;11:1–10. https://doi.org/10.1186/S13018-016-0377-Y.
[44] Eberle S, Gerber C, Von Oldenburg G, Hungerer S, Augat P. Type of hip fracture determines load share in intramedullary osteosynthesis. Clin Orthop Relat Res 2009;467:1972–80. https://doi.org/10.1007/s11999-009-0800-3.
[45] Eberle S, Göttlinger M, Augat P. Individual density-elasticity relationships improve accuracy of subject-specific finite element models of human femurs. J Biomech 2013;46:2152–7. https://doi.org/10.1016/j.jbiomech.2013.06.035.
[46] Cristofolini L. Validation of finite element models. In: Simpson H, Augat P, editors. Experimental research methods in orthopedic and trauma. Stuttgart, New York, Delhi: Rio: Thieme Publishing Group; 2015. p. 156–66.
[47] Henninger HB, Reese SP, Anderson AE, Weiss JA. Validation of Computational Models in Biomechanics. Proc Inst Mech Eng H 2010;224:801–12. https://doi.org/10.1038/jid.2014.371.
[48] Szpalski M, Gunzburg R, Aebi M, Delimoge C, Graf N, Eberle S, et al. A new approach to prevent contralateral hip fracture: evaluation of the effectiveness of a fracture preventing implant. Clin Biomech 2015;30:713–19. https://doi.org/10.1016/j.clinbiomech.2015.05.001.
[49] Varga P, Grünwald L, Inzana JA, Windolf M. Fatigue failure of plated osteoporotic proximal humerus fractures is predicted by the strain around the proximal screws. J Mech Behav Biomed Mater 2017;75:68–74. https://doi.org/10.1016/j.jmbbm.2017.07.004.
[50] Lee TC, Huang HT, Lin YC, Chen CH, Cheng YM, Chen JC. Bicondylar tibial plateau fracture treated by open reduction and fixation with unilateral locked plating. Kaohsiung J Med Sci 2013;29:568–77. https://doi.org/10.1016/j.kjms.2013.01.006.
[51] Gosling T, Schandelmaier P, Muller M, Hankemeier S, Wagner M, Krettek C. Single lateral locked screw plating of bicondylar tibial plateau fractures. Clin Orthop Relat Res 2005;439:207–14. https://doi.org/10.1097/01.blo.0000176147.31756.4c.
[52] Kim CW, Lee CR, An KC, Gwak HC, Kim JH, Wang L, et al. Predictors of reduction loss in tibial plateau fracture surgery: Focusing on posterior coronal fractures. Injury 2016;47:1483–7. https://doi.org/10.1016/j.injury.2016.04.029.
[53] Chen F, Huang X, Ya Y, Ma F, Qian Z, Shi J, et al. Finite element analysis of intramedullary nailing and double locking plate for treating extra-articular proximal tibial fractures. J Orthop Surg Res 2018;13:1–8. https://doi.org/10.1186/s13018-017-0707-8.
[54] Luo CA, Hwa SY, Lin SC, Chen CM, Tseng CS. Placement-induced effects on high tibial osteotomized construct - biomechanical tests and finite-element analyses. BMC Musculoskelet Disord 2015;16:1–10. https://doi.org/10.1186/s12891-015-0630-2.
[55] Duda GN, Mandruzzato F, Heller M, Goldhahn J, Moser R, Hehli M, et al. Mechanical boundary conditions of fracture healing: borderline indications in the treatment of unreamed tibial nailing. J Biomech 2001;34:639–50. https://doi.org/10.1016/S0021-9290(00)00237-2.
[56] Kutzner I, Heinlein B, Graichen F, Bender A, Rohlmann A, Halder A, et al. Loading of the knee joint during activities of daily living measured in vivo in five subjects. J Biomech 2010;43:2164–73. https://doi.org/10.1016/j.jbiomech.2010.03.046.
[57] Chong ACM, Friis EA, Ballard GP, Czuwala PJ, Cooke FW. Fatigue performance of composite analogue femur constructs under high activity loading. Ann Biomed Eng 2007;35:1196–205. https://doi.org/10.1007/s10439-007-9284-z.
[58] Chong ACM, Miller F, Buxton M, Friis EA. Fracture toughness and fatigue crack propagation rate of short fiber reinforced epoxy composites for analogue cortical bone. J Biomech Eng 2007;129:487–93. https://doi.org/10.1115/1.2746369.

9. References

1. Pätzold R, Friederichs J, von Rüden C, et al (2017) The pivotal role of the coronal fracture line for a new three-dimensional CT-based fracture classification of bicondylar proximal tibial fractures. Injury 48:2214–2220. https://doi.org/10.1016/j.injury.2017.06.019

2. Lee TC, Huang HT, Lin YC, et al (2013) Bicondylar tibial plateau fracture treated by open reduction and fixation with unilateral locked plating. Kaohsiung J Med Sci 29:568–577. https://doi.org/10.1016/j.Kjms.2013.01.006

3. Eggli S, Hartel MJ, Kohl S, et al (2008) Unstable bicondylar tibial plateau fractures: A clinical investigation. J Orthop Trauma 22:673–679. https://doi.org/10.1097/BOT.0b013e31818b1452

4. Xie X, Zhan Y, Wang Y, et al (2020) Comparative analysis of mechanism-associated 3-dimensional tibial plateau fracture patterns. J Bone Joint Surg Am 102:410–418. https://doi.org/10.2106/JBJS.19.00485

5. Chang SM, Hu SJ, Zhang YQ, et al (2014) A surgical protocol for bicondylar four-quadrant tibial plateau fractures. Int Orthop 38:2559–2564. https://doi.org/10.1007/s00264-014-2487-7

6. Barei DP, O'Mara TJ, Taitsman LA, et al (2008) Frequency and fracture morphology of the posteromedial fragment in bicondylar tibial plateau fracture patterns. J Orthop Trauma 22:176–182. https://doi.org/10.1097/BOT.0b013e318169ef08

7. Weaver MJ, Harris MB, Strom AC, et al (2012) Fracture pattern and fixation type related to loss of reduction in bicondylar tibial plateau fractures. Injury 43:864–869. https://doi.org/10.1016/j.injury.2011.10.035

8. Hu YL, Ye FG, Ji AY, et al (2009) Three-dimensional computed tomography imaging increases the reliability of classification systems for tibial plateau fractures. Injury 40:1282–1285. https://doi.org/10.1016/j.injury.2009.02.015

9. Hackl W, Riedl J, Reichkendler M, et al (2001) [Preoperative computerized tomography diagnosis of fractures of the tibial plateau]. Unfallchirurg 104:519–523. https://doi.org/10.1007/s001130170115

10. Jiang R, Luo CF, Wang MC, et al (2008) A comparative study of Less Invasive Stabilization System (LISS) fixation and two-incision double plating for the treatment of bicondylar tibial plateau fractures. Knee 15:139–143. https://doi.org/10.1016/j.knee.2007.12.001

11. Lindeque B, Baldini T (2010) A biomechanical comparison of three different lateral tibia locking plates. Orthopedics 33:18–21. https://doi.org/10.3928/01477447-20091124-25

12. Barei DP, Nork SE, Mills WJ, et al (2004) Complications associated with internal

fixation of high-energy bicondylar tibial plateau fractures utilizing a two-incision technique. J Orthop Trauma 18:649–657. https://doi.org/10.1097/00005131-200411000-00001

13. Higgins TF, Kemper D, Klatt J (2009) Incidence and morphology of the posteromedial fragment in bicondylar tibial plateau fractures. J Orthop Trauma 23:45–51. https://doi.org/10.1097/BOT.0b013e31818f8dc1

14. Pätzold R, Spiegl U, Wurster M, et al (2013) [Proximal tibial fractures sustained during alpine skiing - Incidence and risk factors]. Sportverletz Sportschaden 27:207–211. https://doi.org/10.1055/s-0033-1356108

15. Berkson EM, Virkus WW (2006) Hi-energy tibial plateau fractures. J Am Acad Orthop Surg 14:20–31. https://doi.org/10.5435/00124635-200601000-00005

16. Kfuri M, Schatzker J (2018) Revisiting the Schatzker classification of tibial plateau fractures. Injury 49:2252–2263. https://doi.org/10.1016/j.injury.2018.11.010

17. Barei DP, Nork SE, Mills WJ, et al (2006) Functional outcomes of severe bicondylar tibial plateau fractures treated with dual incisions and medial and lateral plates. J Bone Joint Surg Am 88:1713–1721. https://doi.org/10.2106/JBJS.E.00907

18. Ali AM, Saleh M, Bolongaro S, et al (2006) Experimental model of tibial plateau fracture for biomechanical testing. J Biomech 39:1355–1360. https://doi.org/10.1016/j.jbiomech.2005.03.022

19. Mueller KL, Karunakar MA, Frankenburg EP, et al (2003) Bicondylar tibial plateau fractures: A biomechanical study. Clin Orthop Relat Res 412:189–195. https://doi.org/10.1097/01.blo.0000071754.41516.e9

20. Lasanianos NG, Garnavos C, Magnisalis E, et al (2013) A comparative biomechanical study for complex tibial plateau fractures: Nailing and compression bolts versus modern and traditional plating. Injury 44:1333–1339. https://doi.org/10.1016/j.injury.2013.03.013

21. Gösling T, Schandelmaier P, Marti A, et al (2004) Less invasive stabilization of complex tibial plateau fractures: A biomechanical evaluation of a unilateral locked screw plate and double plating. J Orthop Trauma 18:546–551. https://doi.org/10.1097/00005131-200409000-00011

22. Hackl W, Riedl J, Reichkendler M, et al (2001) [Preoperative computerized tomography diagnosis of fractures of the tibial plateau]. Unfallchirung 104:519–523. https://doi.org/10.1007/s001130170115

23. Chan PS, Klimkiewicz JJ, Luchetti WT, et al (1997) Impact of CT scan on treatment plan and fracture classification of tibial plateau fractures. J Orthop Trauma 11:484–489. https://doi.org/10.1097/00005131-199710000-00005

24. Luo CF, Sun H, Zhang B, et al (2010) Three-column fixation for complex tibial plateau fractures. J Orthop Trauma 24:683–692. https://doi.org/10.1097/BOT.0b013e3181d436f3

25. Krause M, Preiss A, Müller G, et al (2016) Intra-articular tibial plateau fracture characteristics according to the “Ten segment classification”. Injury 47:2551–2557. https://doi.org/10.1016/j.injury.2016.09.014

26. Part-Fabregat S, Camacho-Carrasco P (2017) Treatment strategy for tibial plateau fractures: an update. EFORT Open Rev 1:225–232. https://doi.org/10.1302/2058-5241

27. Millar SC, Arnold JB, Thewlis D, et al (2018) A systematic literature review of tibial plateau fractures: What classifications are used and how reliable and useful are they? Injury 49:473–490. https://doi.org/10.1016/j.injury.2018.01.025

28. Gösling T, Schandelmaier P, Marti A, et al (2004) Less invasive stabilization of complex tibial plateau fractures: A biomechanical evaluation of a unilateral locked screw plate and double plating. J Orthop Trauma 18:546–551. https://doi.org/10.1097/00005131-200409000-00011

29. Ali AM, Saleh M, Bolongaro S, et al (2003) The strength of different fixation techniques for bicondylar tibial plateau fractures-- A biomechanical study. Clin Biomech 18:864–870. https://doi.org/10.1016/S0268-0033(03)00149-9

30. Higgins TF, Klatt J, Bachus KN (2007) Biomechanical analysis of bicondylar tibial plateau fixation: How does lateral locking plate fixation compare to dual plate fixation? J Orthop Trauma 21:301–306. https://doi.org/10.1097/BOT.0b013e3180500359

31. Dougherty PJ, Kim DG, Meisterling S, et al (2008) Biomechanical comparison of bicortical versus unicortical screw placement of proximal tibia locking plates: A cadaveric model. J Orthop Trauma 22:399–403. https://doi.org/10.1097/BOT.0b013e318178417e

32. Horwitz DS, Bachus KN, Craig MA, et al (1999) A biomechanical analysis of internal fixation of complex tibial plateau fractures. J Orthop Trauma 13:545–549. https://doi.org/10.1097/00005131-199911000-00005

33. Wu CC, Tai CL (2007) Plating treatment for tibial plateau fractures: A biomechanical comparison of buttress and tension band positions. Arch Orthop Trauma Surg 127:19–24. https://doi.org/10.1007/s00402-006-0192-8

34. Ali AM, Yang L, Hashmi M, et al (2001) Bicondylar Tibial plateau fractures managed with the Sheffield Hybrid fixator. Biomechanical study and operative technique. Injury 32:SD86-91. https://doi.org/10.1016/s0020-1383(01)00165-6

35. Watson JT, Ripple S, Hoshaw SJ, et akl (2002) Hybrid external fixation for tibial plateau fractures: Clinical and biomechanical correlation. Orthop Clin North Am 33:199–209. https://doi.org/10.1016/S0030-5898(03)00080-4

36. Egol KA, Su E, Tejwani NC, et al (2004) Treatment of complex tibial plateau fractures using the less invasive stabilization system plate: Clinical experience and a laboratory comparison with double plating. J Trauma 57:340–346. https://doi.org/10.1097/01.TA.0000112326.09272.13

37. Yoo BJ, Beingessner DM, Barei DP (2010) Stabilization of the posteromedial fragment

in bicondylar tibial plateau fractures: A mechanical comparison of locking and nonlocking single and dual plating methods. J Trauma 69:148–155. https://doi.org/10.1097/TA.0b013e3181e17060

38. Kluess D (2010) Finite element analysis in orthopaedic biomechanics. In: Moratal D (ed) Finite element analysis. Intech Open, pp 151–171. https://doi.org/10.1016/j.mporth.2012.10.007

39. Yosibash Z (2015) Principles of finite elements analysis. In: Simon H, Augat P (ed) Experimental research methods in orthopedics and trauma, 1st ed. Stuttgart, New York, Delhi: Rio: Thieme Publishing Group, pp 145–155. https://doi.org/10.1055/b-0035-122020

40. Kluess D, Souffrant R, Mittelmeier W, et al (2009) A convenient approach for finite-element-analyses of orthopaedic implants in bone contact: Modeling and experimental validation. Comput Methods Programs Biomed 95:23–30. https://doi.org/10.1016/j.cmpb.2009.01.004

41. Henninger HB, Reese SP, Anderson AE, et al (2010) Validation of computational models in biomechanics. Proc Inst Mech Eng H 224:801–812. https://doi.org/10.1243/09544119JEIM469

42. Cristofolini L (2015) Validation of finite element models. In: Simpson, Hamish; Augat P (ed) Experimental research methods in orthopedics and trauma, 1st ed. Stuttgart, New York, Delhi: Rio: Thieme Publishing Group, pp 145–155. https://doi.org/10.1055/b-0035-122020

43. Huang X, Zhi Z, Yu B, et al (2015) Stress and stability of plate-screw fixation and screw fixation in the treatment of Schatzker type IV medial tibial plateau fracture: A comparative finite element study. J Orthop Surg Res 10:1–9. https://doi.org/10.1186/s13018-015-0325-2

44. Carrera I, Gelber PE, Chary G, et al (2016) Fixation of a split fracture of the lateral tibial plateau with a locking screw plate instead of cannulated screws would allow early weight bearing: A computational exploration. Int Orthop 40:2163–2169. https://doi.org/10.1007/s00264-015-3106-y

45. Chen P, Lu H, Shen H, et al (2017) Newly designed anterolateral and posterolateral locking anatomic plates for lateral tibial plateau fractures: A finite element study. J Orthop Surg Res 12:1–9. https://doi.org/10.1186/s13018-017-0531-1

46. Belaid D, Germaneau A, Bouchoucha A, et al (2017) Finite element analysis of mechanical behavior of stabilization techniques for tibial plateau fractures. Comput Methods Biomech Biomed Engin 20:13–14. https://doi.org/10.1080/10255842.2017.1382837

47. Chen F, Wu S, Zhong Z, et al (2018) Stress and stability of newly designed medial anatomic locking plates and traditional fixations in the treatment of posterointernal tibial plateau fracture: A comparative finite element study. Int J Clin Exp Med 11:12956–12963

48. Henschel J, Eberle S, Augat P (2016) Load distribution between cephalic screws in a dual lag screw trochanteric nail. J Orthop Surg Res 11:1–10. https://doi.org/10.1186/S13018-016-0377-Y

49. Eberle S, Gerber C, Von Oldenburg G, et al (2009) Type of hip fracture determines load share in intramedullary osteosynthesis. Clin Orthop Relat Res 467:1972–1980. https://doi.org/10.1007/s11999-009-0800-3

50. Eberle S, Göttlinger M, Augat P (2013) Individual density-elasticity relationships improve accuracy of subject-specific finite element models of human femurs. J Biomech 46:2152–2157. https://doi.org/10.1016/j.jbiomech.2013.06.035

51. Yoo BJ, Beingessner DM, Barei DP (2010) Stabilization of the posteromedial fragment in bicondylar tibial plateau fractures: A mechanical comparison of locking and nonlocking single and dual plating methods. J Trauma 69:148–155. https://doi.org/10.1097/TA.0b013e3181e17060

52. Garnavos C (2014) Retropatellar nailing and condylar bolts for complex fractures of the tibial plateau: Technique, pilot study and rationale. Injury 45:1099–1104. https://doi.org/10.1016/j.injury.2014.01.008

10. Acknowledgement

I would like to thank the following persons, without whom I would not have been able to accomplish the long journey of this research, and without whom I would not have made it through my Ph.D. degree. The Biomechanics team at Murnau Trauma Center, particularly to my supervisor Prof. Peter Augat, whose professional insight and knowledge into the subject matter steered me through this challenging investigation. Also, special thanks to Dr. Robert Pätzold, Dr. Sven Herrmann, and Mr. Martin Winkler, whose heartwarming collaborations allowed my studies to go the extra miles. In addition, I wish to acknowledge Prof. Peter Müller and Dr. Yan Chevalier from Department of Orthopedic Surgery, Physical Medicine and Rehabilitation, University Hospital of Munich (LMU) for their supervisions. Furthermore, my biggest thanks to DAAD organization regarding their scholarship program which provided me a great opportunity to execute my Ph.D. studies in Germany. Moreover, it is worth to be grateful for the institutional supports of Stryker company as well as editor sections of "Archives of Orthoaedic Trauma Surgey" and "Medical Engineering and Physics" Journals regarding publication of this study outcomes. Importantly, I wish to extend my special thanks to my beloved family for all of their emotional support. The words are powerless to appreciate their invaluable incentives which assisted me to industriously pass this academic path in order to accomplish the four years of the highest academic degree.